4

Vacancy drag: A model for kinetics of the interface on the nanoscale

4.1 Introduction and summary

In the previous two chapters, I have investigated interfacial motion in the normal grain growth and in the presence of secondary-phase particles from a macroscopic perspective. In this chapter dynamics of interface with more concerns about its atomistic structure are considered.

The geometric properties of interfaces in polycrystalline materials are usually imposed by production history of the grains, e.g. solidification, cold work, heat treatment, etc. Thereafter, the grains have very little chance to move and adjust to the constrained surroundings. Hence the atoms located at the boundaries barely fit to the space between the grains and there are localized free volumes at the interfaces. High diffusivity, high electrical resistivity, high chemical activity and toughness are general properties related to the irregularity and distortion at the grain boundaries.

Corresponding to the free volumes at the interface, there are local elastic strains which may restrict the motion of the interface. One mechanism to relax the mechanical distortion is adsorbing (or emitting) mobile defects such as vacancies. A vacancy is a structural point defect of removing one atom from the lattice which carries small amount of strain. It is also the key element of self-diffusion.

Solute atoms are also able to interact with interfaces and influence their migration[1] either chemically or mechanically. Diffusion-induced interface motion is reported for some metallic polycrystalline materials in which accumulation of solute atoms at the interface motivates its migration. For the first time, Hillert and Purdy [82] reported this effect for the Fe-Zn system. The mechanism of this effect is widely studied. Hillert [83] and Penrose [84] discussed an elastic mechanism related to the lattice misfit between solute and solvent in which, the mechanical driving force is proportional to squared of concentration difference between the two sides of the interface, while Balluffi and Cahn

---

[1] Vacancies can be imagined as a secondary element (solute) within a pure substance.

[85] proposed that the difference in diffusion coefficients at the interface is responsible for diffusion-induced migration of the interface.

Another study by Schmitz et al. [86] has shown that in a diffusion-couple, the order of layering may cause stresses which influence the diffusion rates: they have deposited nanosized Al/Cu/Al and Cu/Al/Cu layers on a finger tip of about 50 nm in diameter (curved geometry) and observed a significant imbalance of vacancy concentration existing in different layers. Owing to the geometry and small size of the system the internal stresses have been produced which lead to an asymmetric diffusion process in the system [86, 87].

In this chapter a pure nanocrystalline substance in which vacancies will be the only present point defects is considered. In Ns materials, the population of interfaces is very high and their free volumes no longer can be neglected. The interdependency between diffusion of vacancies and the stress build around the interfaces is taken into account and a phase-field model for the phenomenon of nanograin growth is constructed. The description of this model was first proposed by Steinbach et al. [88]. The effect of internal stress on the diffusion in solids, indeed, has been developed by Larche and Cahn [34] and Khachaturian [35] and later has been used in different studies such as nucleation and growth of precipitates [89, 90].

The mechanical stresses can modify the diffusion mechanism in two ways: i) if the species create lattice distortions or ii) if the elastic constants are concentration-dependent, the diffusion can be driven by stress/strain gradients such that the total elastic strain is reduced. This is a delicate interdependency between concentration and stress fields. In the first case, the “mobile eigenstrains” compensate each other or any other source of distortion by means of diffusion. In a dynamic system consisting of many sinks and sources of distortion, this can lead to a complex trajectory of atoms and microstructural changes. In the second case, materials respond to the mechanical stress by local softening and hardening which is controlled by diffusion of suited species.

In the following parts, I first give an overview about properties of Ns polycrystalline materials. Before introducing the methods, I briefly summarize the thermodynamic and mechanical characteristics of vacancies which seems necessary for our future reference. The results of the model are presented and compared with the background of other relevant models and experimental studies. In the present model, the dynamic of the interface is tuned by natural cooperation of the curvature, mechanical energy due to free volumes, and diffusion of vacancies. The curvature-driven motion of the interfaces is hindered by mechanical distortion. In order to unlock the interfaces, the interfacial distortion should be relaxed by diffusion of vacancies. Thereupon, there are two competitive kinetic processes, namely, the curvature-driven motion and the diffusion of vacancies which determine the kinetics of growth. Diffusion-controlled growth is found to be dominant on the nanoscale, specially at low temperatures.

4.2 Nanocrystalline materials

The object of study in this chapter is the contribution of diffusion (vacancies) to the grain growth in the presence of internal stress gradients. This is directly related to the nanocrystallined bulk materials which usually contain a large amount of defects and distortion. In this section, I briefly review the definition, properties and relevant findings about these special materials.

In the recent decades, Ns materials with an average grain size of less than 0.1 μm have been considered as new possibilities for achieving better mechanical and functional properties [91, 92, 93, 94, 95]. The interfacial volume in Ns materials can reach up to 50 % of the total volume and the density at the interfaces may drop to 70 %. A typical 5nm-radius metallic grain contains only about 10,000 atoms. This grain may show a very different behaviour from a conventional grain with 1 μm radius. For instance, the bulk of the nanograins is so small that there would be no source of dislocations to activate the slip systems under stress. Instead of that, the grain may compensate the external stress via rotation to a certain extent. The fabrication of Ns materials causes some side effects on the behaviour of grain boundaries as well [95, 96]. For example, mechanical procedures, such as mechanical alloying, induce a considerable amount of structural defects in atomistic and micro- levels which can influence following processes such as sintering or shaping.

The large amount of point defects and interfaces provides short-circuits which enhance the overall self-diffusion process. At room temperature, the self-diffusion for Ns copper is reported to be about 10^{10} and 10^{4} times larger than bulk and grain boundary diffusion, respectively. Increasing the temperature, the differences will be slightly less, but still significant [94]. It is likely that the large number of triple junctions also play an important role in the self-diffusion mechanism. Solutes, however, may diffuse differently. Since there is a large amount of interfaces, the adsorption capacity is significantly high (high solute solubility) and the solute atoms may be easily trapped. However, once the adsorption sites are occupied at high concentration of solutes, the solute diffusivity may increase. It is even observed that once the concentration at the interfaces are high, the diffusion of solutes may propel the interface [82]. This is called diffusion-induced motion.

Grain size in polycrystalline materials strongly influences their mechanical properties. The smaller the grain size, the stronger the materials is expected. At the nanoscale, however, this is accounted to be inverse below a certain size. This effect, known as inverse Hall–Petch effect, is attributed to sliding at the grain boundary instead of slip systems and also the lack of dislocations. Disordered arrangement of atoms at the interface may also change the heat transfer and heat capacity of these materials. It is reported that the heat capacity of some nanocrystallined materials, such as palladium and copper, is more than corresponding conventional bulk material. For more information the reader is referred to [94, 95].

To apply nanomaterials, the stability of microstructure at desired temperatures must be warranted. The grain growth in nanocrystallines, however, differs from corresponding coarse-grained bodies [6, 97, 98, 99]. The obscure and unpredictable microstructural evolution in Ns materials requires solid studies to uncover the origins of nanograin growth.

Different studies report a broad spectrum of observations concerning nanograin growth. Isothermal annealing experiments revel a slow linear growth regime at low temperatures that changes to normal grain growth above a certain temperature [6, 100]. In order to investigate this abnormality, theoretical models and simulations have been developed that consider grain rotation [101], triple junctions drag [102, 103] or vacancy generation [104, 105] during the growth process. These models have been applied successfully to explain particular experimental observations; however, a full understanding of linear grain growth on the nanoscale still needs for further studies.

4.3 About vacancies

4.3.1 Thermodynamic of vacancies

The minimization of total energy implies that vacancies exist at thermodynamic equilibrium in any atomistic configuration. For the simplest case of pure metals, omitting the vacancy-vacancy interactions, the enthalpy and entropy variation due to adding vacancies will be,

$$\Delta H = X_v \Delta H_v \tag{4.1}$$

and

$$\Delta S = X_v \Delta S_v + R_g \left(X_v \mathrm{ln} X_v + (1 - X_v) \mathrm{ln}(1 - X_v) \right), \tag{4.2}$$

where X_v is the molar fraction of vacancies, ΔH_v is the increase in enthalpy and ΔS_v is thermal increase in entropy per unit of mole of vacancies. At the equilibrium,

$$\frac{dG}{dX_v} = 0, \tag{4.3}$$

where $G = G_0 + \Delta H - T\Delta S$ is the Gibbs energy function. Thus, one obtains the equilibrium concentration of vacancies as,

$$X_v^{eq} = \exp\left(\frac{-\Delta S_v}{R_g}\right) \exp\left(\frac{-\Delta H_v}{R_g T}\right). \tag{4.4}$$

The first term in right-hand side is a temperature-independent constant almost equal to 3 for metals. The second term, however, significantly increases with temperature and close to the melting temperature, vacancy concentration may rise up to 10^{-3}. In reality, however, the concentration of vacancies is usually non-equilibrium. This is due to the existence of defect sources and sinks which can produce vacancies or annihilate them. For instance, vacancies may be generated during removal of grain boundaries which will be discussed later in this chapter. Another possible source for extra vacancies are micro-voids which are formed during non-equilibrium production processes such as severe deformation or sintering.

4.3.2 Strains related to the vacancies

A vacancy maintains usually an empty volume which is smaller than that of a single atom and causes a small volumetric distortion in the lattice. Assuming vacancies to be the secondary element in the crystalline's lattice and apply Vegard's law, the elastic strain corresponding to the vacancies is given,

$$\epsilon_v^{ij} = \frac{a_v - a_l}{a_l} c_v \delta^{ij}, \tag{4.5}$$

with a_v and a_l being vacancy and substance lattice parameters respectively, c_v the local vacancy concentration and δ^{ij} the Kronecker symbol. In the presence of stress gradient, vacancies are able to move. This produces a micro-flow of atoms like it happens during creep. In general, vacancies influence the bond strength of materials and can change the elastic constants of materials as well [106]. In the following studies I focus on the interdependency of vacancies and mechanical properties only through respective eigenstrain variations.

4.3.3 Vacancy generation

Vacancies are thermally enhanced defects. Their existence can be prescribed as natural response of lattice against increasing volume, decreasing pressure or increasing temperature. Vacancies may also be created due to phase transition or any other structural changes which are accompanied with local volume changes. Estrin et al. [107] have pointed that the reduction of grain boundary area during grain growth may cause considerable release of vacancies. They calculate the rate of total free energy change during this event,

$$\dot{G} = -\frac{3\sigma}{2\bar{R}^2}V + \frac{NkT}{c^{eq}}(c - c^{eq})\dot{c}, \tag{4.6}$$

where σ is the interfacial free energy, $\bar{R}$ is the average grain size, V the interfacial velocity and c^{eq} the equilibrium vacancy concentration. The first term is related to interfacial changes and the second one is the excess free energy rate due to excess vacancy concentration $(c - c^{eq})$. Grain growth continues only if $\dot{G} < 0$. They have obtained the rate of concentration change as,

$$\dot{c} = \frac{6\varepsilon\eta}{\bar{R}^2}V - \frac{D_v}{d^2}(c - c_{sink}) \tag{4.7}$$

where ε is relative excess volume of interfaces, η is interfacial thickness, D_v is the vacancy diffusivity, d is sink spacing and c_{sink} is vacancy concentration at the sinks. They propose some other grain boundaries as th sinks. The first term in the right hand side express vacancy generation and the second term gives the vacancy removal rate. The solution for Equation 4.7 is approximated as,

$$c = c_i + \frac{6\varepsilon\eta V}{\bar{R}^2}t, \tag{4.8}$$

where c_i is initial vacancy concentration in bulk. Substituting this equation into Equation 4.6 complete the calculations:

$$\dot{G} = -\frac{\sigma}{\bar{R}^2}V + 24\left(\frac{\varepsilon\eta V}{\bar{R}^2}\right)^2\frac{NkT}{c^{eq}}t < 0. \tag{4.9}$$

Inequality 4.9 says that vacancy generation increases the total free energy of the system. Therefore, above a certain time t^* grain growth is stagnated. Thereafter, the system needs some time for redistributing the excess vacancies. In reality both of these phenomena happen simultaneously which results in new kinetics which is observed in related structures, e.g. Ns materials.

4.4 The model for interaction between interfaces and vacancies

I already mentioned that vacancies maintain a small amount of free volume and distortion. Thus, the local density of atoms varies slightly from place to place within the substance. Assigning an unite volume to each atom it is possible to express the free volumes in terms of concentration. Considering a pure substance, one can define vacancy $c_v(x,t)$ and atoms $c_a(x,t)$ concentration fields with,

$$c_v(x,t) + c_a(x,t) = c_{v0}(x,t) + c_{a0}(x,t) = 1. \tag{4.10}$$

$c_{v0}(x,t)$ and $c_{a0}(x,t)$ are corresponding reference values[1]. Equation 4.5 maintains for the concentration field,

$$\epsilon_v^{ij} = \frac{a_v - a_l}{a_l} c_v(x,t)\delta^{ij}. \tag{4.11}$$

On the other hand, interfaces are attributed by geometrically-required deformations (strain), corresponding to the mismatch between the grains. The amount of the strain is determined by local arrangement of the atoms, but it can be taken as a constant value in average. This deformation represents the free volume at the interface which can be significantly large for nanocrystalline materials as mentioned in Section 4.2. In the phase-field notation interfaces can be specified with a proper function $h_\epsilon(\phi)$ of the phase-field variables. Therefore, one can express distribution of geometrically-required strain as,

$$\epsilon_g^{*ij} = h_\epsilon(\phi)\ \epsilon_g^{0*}\delta^{ij}. \tag{4.12}$$

$h_\epsilon(\phi)$ is a non-zero interfacial function and ϵ_g^{0*} is a constant. The integration over Equation 4.12 will be equal to the ϵ_g (the total interfacial strain) which is set proportional to the total free volume of the interface. $h_\epsilon(\phi) = \phi(1-\phi)$ is chosen. Thus, across a dual interface,

$$\epsilon_g = \epsilon_g^{0*} \int_{-\infty}^{+\infty} \phi(1-\phi)\ dx\ = \frac{\eta}{8}\epsilon_g^{0*}. \tag{4.13}$$

For multiphase contributions I use a linear summation of all dual contributions as,

$$\epsilon_g^{*ij} = \epsilon_g^{0*}\delta^{ij} \sum_{i\neq j} \phi_i\phi_j. \tag{4.14}$$

Summing up above contributions, the total eigenstrain will be $\epsilon_v^{ij} + \epsilon_g^{*ij}$ and the elastic energy density obtains

$$f^{mech} = \frac{1}{2}(\epsilon^{ij} - (\epsilon_v^{ij} + \epsilon_g^{*ij}))\bar{C}^{ijkl}(\epsilon^{kl} - (\epsilon_v^{kl} + \epsilon_g^{*kl})). \tag{4.15}$$

---

[1] At constant volume, the density field $\rho(x,t) = \frac{N_a}{V}$ with a reference density $\rho_0(x,t)$ (for thermodynamically stable bulk phase at a certain temperature) is an identical definition. Thereupon, one obtains $\rho(x,t) = \frac{c_a(x,t)}{V_a} = \frac{1-c_v(x,t)}{V_a}$ where V_a is the volume of a single atom.

This mechanical energy acts against interfacial motion and hinders the growth (See Section 4.5.2). At the equilibrium, however, the interfacial deformation can be compensated with the diffusion of vacancies which means $\epsilon_v^{ij} + \epsilon_g^{*ij} \to 0$. If the mechanical distortion is fully compensated, the motion of the interface will be free from mechanical effects and only curvature-driven.

Once the interface moves, however, the balance between the two sources of the deformation breaks: the geometrically-required deformation tends to move with the interface velocity while vacancies migrates via diffusion.

From the equation of diffusion it is known that atoms always flow in a manner which would decrease the chemical potential gradient,

$$j = M_a \nabla \mu, \tag{4.16}$$

where M_a is the atomistic mobility and $\mu = \frac{\delta F}{\delta c}$ is the Gibbs chemical potential. This equation implies that the flux goes to zero if the chemical potential becomes equal everywhere. Here F is the total free energy functional which the elastic energy is a subset of that. Substituting Equation 4.15 into Equation 4.16 one obtains the flux of vacancies driven by elastic energy heterogeneities,

$$j = M_a \nabla \left(\frac{\delta f^{mech}}{\delta c_v} \right) = M_a \nabla \left(\frac{a_v - a_l}{a_l} \delta^{ij} \bar{C}^{ijkl} (\epsilon^{kl} - (\epsilon_v^{kl} + \epsilon_g^{*kl})) \right). \tag{4.17}$$

This equation demonstrates that the gradient of hydrostatic stress produces a *mechanochemical potential* which drives vacancies. In other words, vacancies will migrate in the stressed region around a moving interface seeking mechanical relaxation around the interface ($\frac{\delta f^{mech}}{\delta c_v} \to 0$). In the simulations, I treat density variation with a concentration field $c_v(x,t)$, which express the local free volume, and solve its time-variation,

$$\dot{c} = \nabla . j = M_a \frac{a_v - a_l}{a_l} \nabla . \nabla \left(\delta^{ij} \bar{C}^{ijkl} (\epsilon^{kl} - (\epsilon_v^{kl} + \epsilon_g^{*kl})) \right). \tag{4.18}$$

The constant M_a is a temperature-dependent quantity equal to atomistic mobility in the bulk material. The Vegard's factor $\frac{a_v - a_l}{a_l}$ may also depend on the temperature, but it is taken as a constant in the current model.

4.4.1 Mechanical solution for interfacial deformations

Existence of the strain in the interface causes elastic stress in the body of the system which can influence different events, such as mass transport phenomena, in a long-range distance within the bulk of the grains. Hence it is important to know about the distribution and amplitude of the stress within the local volume around the interface. For the sake of feasibility for an analytical approach, a single spherical grain embedded in an infinite substrate is considered which is separated from the substrate through a deformed interface. The analytical solutions, given in Appendix B, are plotted in Figure 4.1. Here it is assumed that materials inside, within, and outside the interface are isotropic with the same elastic constants. The interface is expanded volumetrically by 1 % ($\epsilon_B^{*rr} = \epsilon_B^{*\theta\theta} = \epsilon_B^{*\Phi\Phi} = 0.01$).

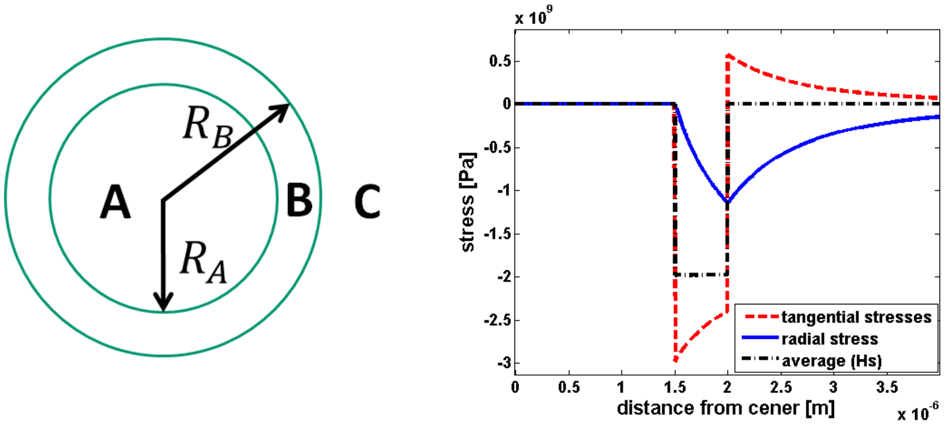

Figure 4.1: Analytical solution for interfacial distortion are shown. Volume B (0.5 μm width and 1 % volumetric expansion) is the interface between grain A (1.5 μm radius) and substrate C. All phases are assumed to have same isotropic elastic constants (Young modulus of 208 GPa). The stress distribution is shown in the graph (right). It is found that there is no stress build in the grain interior due to the interfacial distortion.

Surprisingly, it is found that regardless of its elastic constants, the grain does not feel any stress in this condition. The interface volume is under pressure and the solution within the substrate is similar to the Eshelby solutions (see Section 4.5.1). In other words, the volumetric deformation of the interface does not cause pressure within the grain with isotropic elastic properties.

If the elastic constants of the interface and the substrate are different from each other ($E_B \neq E_C$), the grain (domain A) will also be under stress (Figure 4.2). The source of the pressure inside the grain, indeed, is not the interfacial deformation, but the heterogeneous elastic properties of its surrounding medium. In general, if any obstacle in the interface or substrate interfere to the stress fields, the grain's interior will feel the pressure as well. In the polycrystalline structures, each grain is surrounded with many other grains and grain boundaries which provide the heterogeneous media and result internal stresses inside the grains. It is worth noting that the sign of the stress depends on the sign of the eigenstrains, whether there is expansion of contraction at the interface. The motion of the interfaces is also a source of heterogeneity that significantly contributes to the stress distribution which will be discussed in Section 4.6.1.

4.5 Mechanical contribution in the diffuse interface evolution

In the MPF model, the volume of simulation is considered to be at mechanical equilibrium which assumes mechanical stresses propagate instantaneously through the system. In the following, brief details about the mechanical equilibrium, the mechanical solver, its verifications, and the mechanical driving force related to the model are introduced.

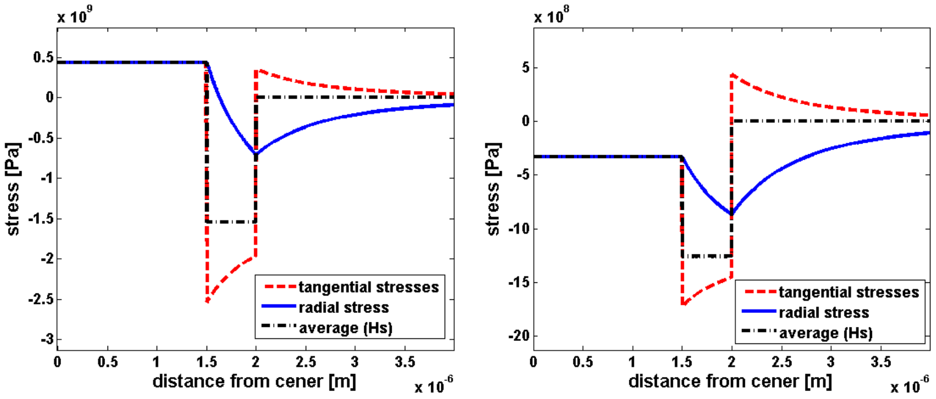

Figure 4.2: Analytical solutions within and around a spherical grain (1 % volumetric expansion at the interface), for softer substrate, $E_B > E_C$, (left), and softer interface, $E_C > E_B$, (right), are shown. The elastic property of the spherical grain do not influence the results.

4.5.1 Eshelby test of spectral mechanical solver

Since an Eulerian method for finite difference volumes is used, it naturally does not allow for expansion or contraction of the simulation box. To get ride of this artificial effect, the volumetric changes of the box should be taken into account. This is done by exploiting an iterative Fast-Fourier Transformation (FFT) method which mimics the volume changes of the simulation box: first the strains are calculated for fixed system, thereafter one subtracts/adds an average volumetric strains (diagonal elements) from/to all discrete volumes iteratively until the total hydrostatic stress over whole box vanishes. This reflects a free boundary system allowed to deform at its surface or equally an infinite medium without stress/strain at far distance. Without this scheme the finite size effect will strongly influence the mechanical equilibrium.

In order to verify applied homogenization scheme over the diffuse interface, as well as the free volume expansion scheme mentioned above, the analytical Eshelby solution for a spherical inclusion of isotropic elasticity to which it is possible to compare the simulation results is considered. Figure 4.3 presents the σ^{11} and σ^{33} in a plane normal to 1 axis (x) for an inclusion of radius 17 nm with 1 % volumetric expansion ($\epsilon^* = 0.01$ along each axis). Both the inclusion and matrix are isotropic with $C^{11} = 289.8$ GPa, $C^{12} = 163.4$ GPa and $\nu = 0.33$ (as reported for pure cobalt). The simulation box is 129 nm on each side and the interface width is 5 nm. Analytical solutions tell us there is a hydrostatic pressure inside the inclusion with constant diagonal elements of,

$$\sigma^{ii} = -\frac{2}{3}\epsilon^*(C^{11} + 2C^{12})\frac{1-2\nu}{1-\nu} \qquad r < R_p. \tag{4.19}$$

R_p is the inclusion radius. Within the matrix and in the chosen plane (perpendicular to axis 1) the stress components are,

$$\sigma^{11} = -2\sigma^{22} = -2\sigma^{33} = -\frac{2}{3}\epsilon^*(C^{11} + 2C^{12})\frac{1-2\nu}{1-\nu}\left(\frac{r}{R_p}\right)^3 \qquad r \geq R_p. \tag{4.20}$$

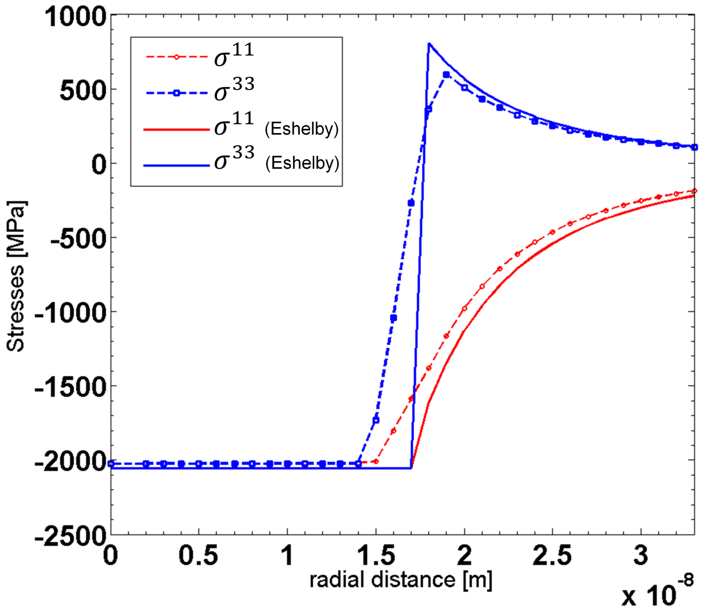

Figure 4.3: Stress distribution around a spherical inclusion with 1 % volumetric expansion.

Outside the interface region and inside the grain, the numerical solutions converge pretty well to the corresponding analytic solutions. Deviation at the interface strongly depends on interfacial width with respect to the size of the inclusion. The tangential stress components are less accurate. The deviation for diagonal elements, however, is still acceptable for our phase-field calculations.

4.5.2 Mechanical driving force

In the phase-field modelling, the contribution of non-interfacial energy terms are separately calculated. This is already discussed in Chapter 1. The general derivation applies for mechanical contributions,

$$\Delta G_{\alpha\beta}^{mech} = -\left(\frac{\partial}{\partial\phi_\alpha} - \frac{\partial}{\partial\phi_\beta}\right) f^{mech}, \tag{4.21}$$

where depending on homogenization scheme, the driving force would be slightly different (See Appendix C). The new model, however is slightly different such that the interfacial area has its own mechanical property. However, this does not influence the mechanical nature of the system. Assuming continuity of stress and displacement all over the space and homogeneity of elasticity, the Voigt homogenization scheme is applied. Therefore,

$$\Delta G_{\alpha\beta}^{mech} = -\epsilon_g^{0*}\delta^{ij}\bar{C}^{ijkl}(\epsilon^{kl} - (\epsilon_v^{kl} + \epsilon_g^{*kl}))(\phi_\alpha - \phi_\beta). \tag{4.22}$$

For the current case, the geometrically-required interfacial eigenstrain is distributed through the diffuse interface such that it has a maximum at the centre and vanishes inside the phases which is adopted to the physical description of a symmetric interface. As a result, the mechanical driving force across the interface shapes with two extrema. The absolute values for the driving force overall is relatively small comparing to the extrema. This produces instabilities at the interface. In order to avoid this, a proper averaging procedure along normal direction of the interface is developed. The details of the averaging method is described in Appendix D.

4.6 Demonstration of the model in the MPF scheme

4.6.1 Shrinkage of a single nanograin

In order to demonstrate the new model introduced in Section 4.4, a single spherical grain embedded into a substrate has been again considered. Having the same material constants everywhere, the interface maintains geometrically-required eigenstrain related to the free volumes and the conventional interfacial energy. The simulation starts from equilibrium, where the geometrically-required eigenstrain at the interface is compensated with the vacancies. The isotropic elastic constants of pure cobalt are taken as $C^{11} = C^{22} = C^{33} = 289.8$ GPa, $C^{12} = C^{13} = C^{23} = 163.4$ GPa and $C^{44} = C^{55} = C^{66} = 63.2$ GPa. The initial concentration at the bulk is 2×10^{-4}. The interface energy is chosen to be 1 Jm^{-2} and the interfacial width is $6\Delta x$ where $\Delta x = 0.2$ nm. The mobility of vacancies is $10^{-25}\mathrm{m}^{-2}\mathrm{J}^{-1}$. Each vacancy is assumed to have 0.9 of the size of an atom, then the Vegard's coefficient will be -0.1. The interfacial mobility, on the other hand, is fixed to 10^{-19} $\mathrm{m}^4\mathrm{J}^{-1}\mathrm{s}^{-1}$. The numerical time step is 0.1 s.

The spectral mechanical solver obtains the mechanical equilibrium and the box expansion as described in Section 4.5.1, in each time step. The condition for relaxation is if the absolute value of hydrostatic pressure is less than 10^3 Pa or the hydrostatic strain is less than 10^{-6}. Then, the diagonal components of stress matrix are embedded into Equation 4.18 and gave the hydrostatic stress gradients and the subsequent concentration increment in that time step.

Figure 4.4 shows the results of this simulation. Initially, the mechanical distortion at the interface are assumed to be fully compensated by diffusin of atoms and vacancies. Here, it is needed to introduce the concept of "mobile atoms" which are in contrast to the vacancies. In other word, where the vacancies diffuse out from, the mobile atoms diffuse in. The number of mobile atoms are equal to the vacancies. But there are many potential mobile atoms, as each vacancy in surrounded by many atoms. We might use this concept in our future discussion.

Indeed, depending on the sign of the geometrically-required eigenstrain at the interface, vacancies may diffuse into or out from the interface. It is important to be understood that the local distribution of stresses can be both positive or negative, regardless of positive eigenstrains at the interface. Since a positive build-in eigenstrain is assigned to the interface, vacancies are needed to diffuse into the interface to compensate them. The sign of the stress, strain and concentration components come out from derivations discussed in the model. The negative sign of the concentration field mentions the absent of vacancies and means a compressed structure (higher density), while the positive value presents the vacancies themselves.

As it is expected the vacancies follow the stress gradient within and around the interface (Figure 4.4). Regarding the direction of the motion, geometrically-required

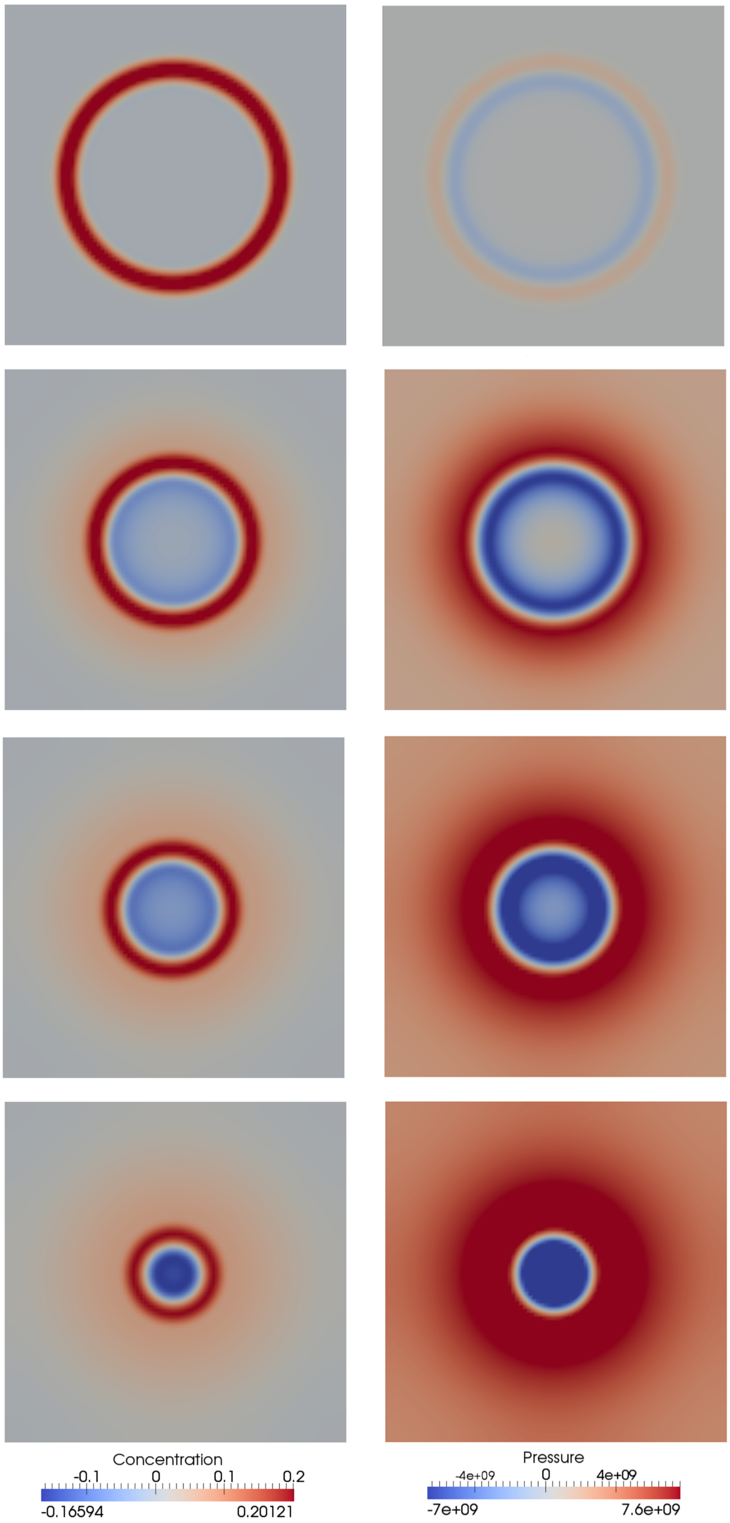

Figure 4.4: Evolution of concentration and pressure fields for a single spherical grain. In front of the moving interface there is a compressed area where the vacancies are adsorbed, while behind the interface, some vacancies are left.

eigenstrains will be annihilated behind the interface while should be build in the front. Thus, in the front of the moving interface vacancies are absorbed to the interface and behind the interface, mobile atoms migrate to compensate the stress. In other words, behind the interface vacancies are pushed to the substrate. Due to shortage of simulation time (small grain) and changing-curvature which varies the total driving force, it is not possible to observe a distinguishable stable motion, where the stress and concentration fields are in balance. The pressure difference inside and outside the grain has a gradient and increases for a shrinking grain. This can be understood also in the frame of local non-equilibrium density difference between the two sides of the interface.

The kinetics of shrinkage is shown in figure 4.5 for different mobility factors. If there would be no diffusion at all, it is seen that the growth is slowed down with the mechanical deformation at the interface which is linear in the period of simulation. In contrast, when the diffusion is considered, the shrinking accelerates. If the mobility of atoms increases, which is possible by means of temperature, the compensation happens faster and eases the motion of the interface. For high enough mobilities the growth happens just same as a normal shrinkage due to the curvature with a parabolic kinetics.

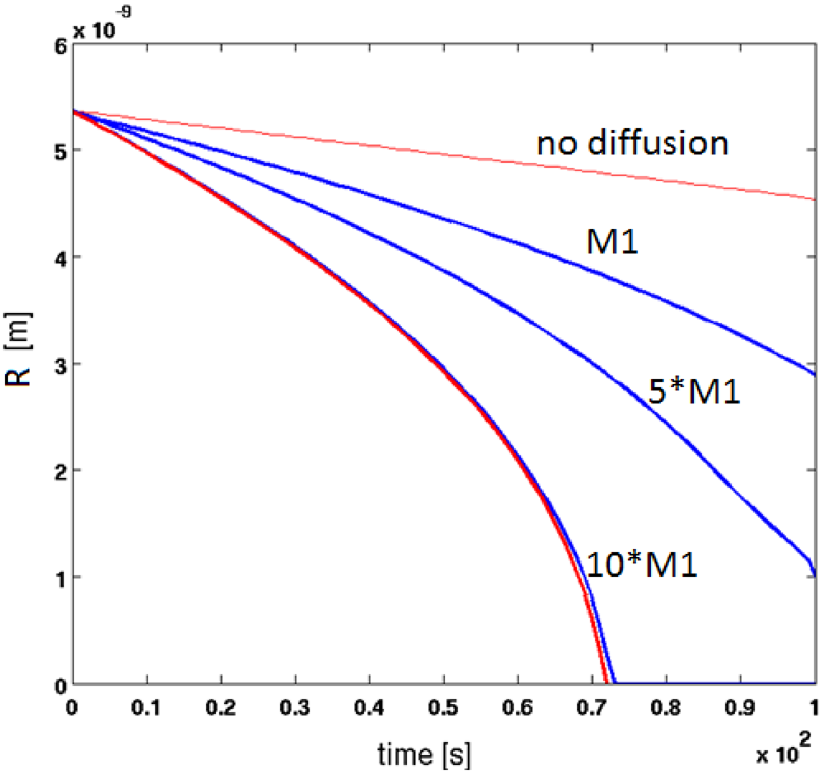

Figure 4.5: The kinetics of shrinkage of a single spherical grain is compared for three different atomic mobilities with M1= 10^{-25}m^{-2}J^{-1}s^{-1} with no diffusion and normal shrinkage cases. At high mobilities the kinetics of shrinkage accelerates and get close to normal shrinkage process.

4.7 Simulation of polycrystalline nanostructured materials

The general procedures of the current simulations are similar to what were previously described in Section 2.5.1. Due to computation costs for mechanical and diffusion solvers the simulation box is limited to 200 grids in each side with a grid spacing of 0.2 nm, and interfacial width of 1.2 nm. A periodic boundary condition is used for the simulation box containing 1000 initial grains with almost the same size. The interfaces were assumed initially to be at mechanical relaxation. The mobility of vacancies M_a is subject to change which reflects the annealing temperature, but the interfacial mobility is kept constant. Other parameters are same as it is described in Section 4.6.1.

4.7.1 Simulation results and discussions

4.7.1.1 Kinetics of nanogrowth

The interfacial energy and the mechanical energy due to the deformation at the interfaces directly contribute into dynamics of the interface. But the diffusion process which influences the total eigenstrains within both the interface and the bulk contributes into the kinetics of the grain growth, indirectly. Figure 4.6 presents the evaluation of average grain size in different systems. The results are presented for the interfaces with 30 % of free volumes. Turning off the diffusion (very low temperature), it can be seen that the growth almost stops. In this case, once the interface wants to move (together with the geometrically-required eigenstrain) a large amount of mechanical energy pills up which hinders the growth. This is where the low speed growth or no growth at all is expected. In this case the interface motion is partially or fully locked by mechanical distortions.

For the atomic mobility a reference value $M_{a0} = 10^{-25}\mathrm{m}^{-2}\mathrm{J}^{-1}\mathrm{s}^{-1}$ is assumed. Simulation results for M_{a0}, $10M_{a0}$ and $100M_{a0}$ are given in Figure 4.6. Once the diffusion turns on, vacancies move at the stress gradients, the eigenstrains compensate and the mechanical distortion at the interfaces can relax. This let the interfaces to move and therefore the growth happens. At this state, the motion of the interface is controlled through both the curvature of the interface and the diffusion of the vacancies. The speed of the interfaces depends on the rate of the diffusion: if the diffusion is slow the bottleneck of the growth kinetics will be vacancy diffusion and the growth is diffusion-controlled. When the atomic mobility is equal to $100M_{a0}$ the mechanical distortions fully compensate at the interfaces and the kinetics of growth almost match with the normal grain growth, which means the growth is again curvature-driven.

The importance of free volume redistribution during grain growth is already mentioned in Sections 4.2 and 4.3. Estrin, Gottstein and Shvindlerman [104, 105, 107] suggested that during the grain growth interfaces release vacancies into the bulk that increases the total free energy of the system and can prevent the growth. Generated vacancies were supposed to diffuse through the bulk to the possible sinks which should be another interfaces. This model has been applied to the grain growth in pure nanocrystalline [7] and thin films [108]. The present work, however, considers another aspect of vacancies which are influenced by the elastic energy potential accumulated at the interface. Shvindlerman [109] and Faulkner explain the thermodynamic of the vacancies at the interfaces where the chemical potential of interface can reduce by adsorption of the vacancies. This is very similar to the concept presented here, except that the

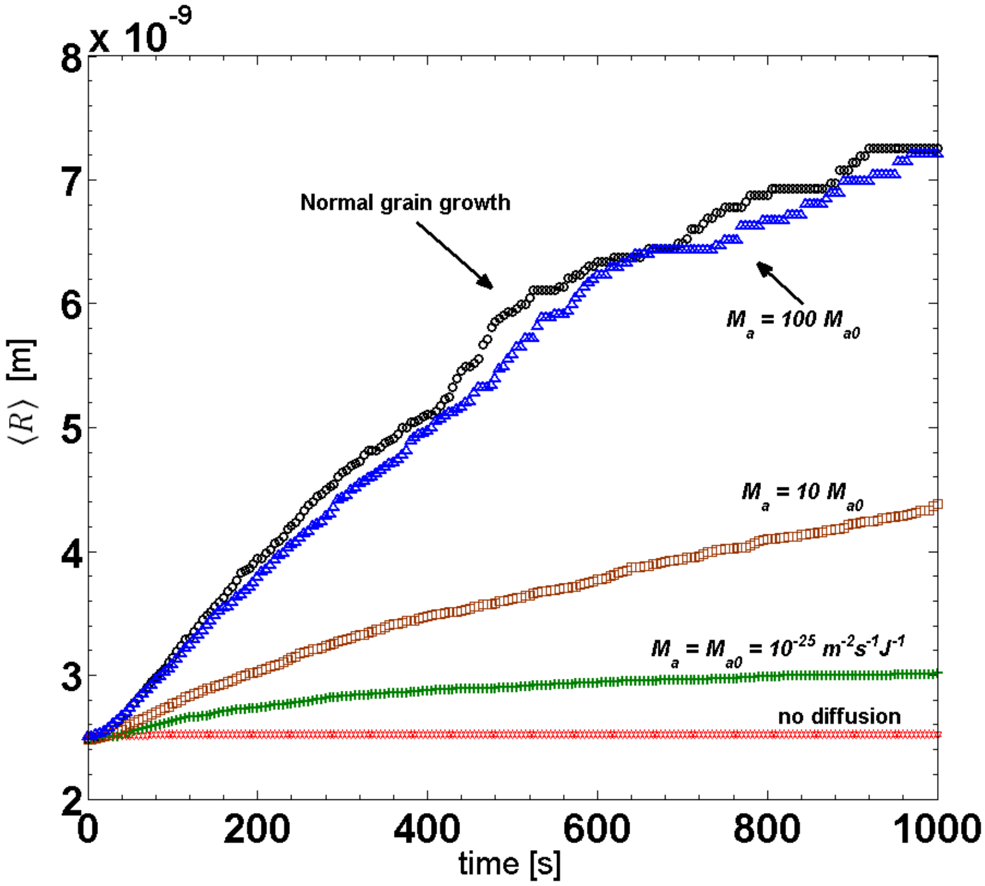

Figure 4.6: Nanocrystallined cobalt are simulated and compared to the normal grain growth of the same system. The grains stop growing if there is no diffusion. For different diffusion rates the kinetics of the growth changes from the diffusion-controlled process to a curvature-driven motion of the interface. The interfaces are considered to have 30 % of free volumes.

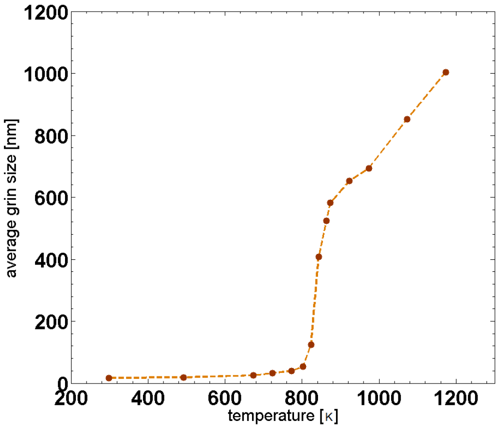

Figure 4.7: The average grain size of pure cobalt nanocrystalline at the end of 1 hour annealing process. The growth mechanism changes at a critical temperature 803 K. Experimental results by Song et al. [6].

mechanical subset of the chemical potential at the interfaces is considered to reduce by gathering of vacancies at deformed interfaces. One advantage of this model over its thermodynamic alternative is that the long-range interaction between interfaces and mobile defects is explained.

In the annealing experiments of nanocrystallined pure cobalt reported by Song et al., the transition from the linear to normal grain growth is observed starting at 803 K is. Estrin et al. [107] suggested a temperature-dependent critical grain size of about 200 nm above which the growth is no more inhibited by vacancy generation and normal grain growth occurs. In the MPF model, although the direct simulation of the transition from linear to normal grain growth is difficult due to abundant computational requirements, the nature of the transition can be discussed as follows. For very small grains, the regular curvature-driven motion would be faster than the maximum velocity allowed by vacancy diffusion. Hence, in this regime, the diffusion-limited motion of interface causes the linear grain growth kinetics. Indeed, the vacancies which move slowly at low temperature impose an indirect drag force on the interface and slow it down. Once the grains reach a critical size above which the curvature contribution to the motion of the interface is lower than the diffusion-controlled kinetics, the controlling mechanism changes. Obviously, the transition size is highly temperature-dependent. For a constant annealing time the grains may not reach the critical grain size at low temperatures which means the growth process is only a linear growth mechanism. In contrast, at high temperatures a fully normal grain growth is expected. Between these two extreme cases, there is a transition range where both linear and normal regimes contribute to the growth process.

The discontinuity on the nanoscale grain growth observed experimentally for pure Co between 800 to 900 K. Figure 4.7 presents the exprimental results obtained by Song et al [6]. The activation energy for migration of vacancies is similar to the self-diffusion activation energy in the bulk of the materials. The self-diffusion in cobalt is expressed in following Arrhenius equation with a large range of temperature [110],

$$D_{Co} = 1.287 \times 10^{-4} \exp\left(\frac{-296542.9}{R_g T}\right) \quad \mathrm{m^2 s^{-1}}. \tag{4.23}$$

Applying Einstein relation –which neglects double-vacancy diffusion and assumes a dilute concentration of vacancies– one obtains,

$$Ma = M_{Co} = \frac{D_{Co}}{R_g T}. \tag{4.24}$$

Thus the corresponding temperatures for M_{a0}, $10M_{a0}$ and $100M_{a0}$ are ≈ 898, ≈ 957 and ≈ 1095 K which are above experimental values. Although the grain size in our simulations are much smaller than reported values in Figure 4.7, it still provides a fair explanation of the possible mechanisms of transition from low-speed grain growth into normal grain growth. From Molecular Dynamics (MD) calculations for copper which were performed parallel to this study in our group [111] we observed that the activation energy of the shrinkage of a single spherical nanograin is about 10% of the activation energy for self-diffusion, this is also reported in some experimental researches [112, 113, 114]. This low activation energy suggests the interfacial diffusion rather than bulk diffusion. In this situation, the speed of the interface is determined by the frequency of atomic jumps across the interfaces. Since we do not assign any special kinetic aspect to the atoms at the interfacial region, the activation energy is everywhere the same which can be one reason for deviation form experimental observations. The MD simulations, however, confirm that the moving interface may leave some vacancies and stacking-fault area (in the case of Cu) behind, which affirm the redistribution of the free volumes.

4.7.1.2 Microstructure and grain size distribution

Figure 4.8 compares the results of two simulation boxes with $10M_{a0}$ and $100M_{a0}$ atomic mobilities. Both simulations start from the same initial structure. Later on, not only they obtain diverse growth kinetics (as shown in figure 4.6), but also the trajectory of microstructural evolution are different. This can be understood because of long-range interactions between diffusion and stress fields. In fact, the flux of atoms in each point of the space may be influenced by more than one interface.

Figure 4.9 shows the concentration and pressure fields at a cross section view for the simulation box with $10M_{a0}$. The location of the interfaces can be easily recognized where the concentration field reaches its minima. Clearly, the concentration of vacancy at the interface is very high. At the triple junctions the concentration is even higher, proportional to the amplitude of deformation. The negative sign for the concentration shows the absent of the vacancies or presence of mobile atoms. This can be interpreted as densification due to pressure. At the beginning, the pressure distribution is very heterogeneous and mostly localized at the interfaces and its adjacent regions. Later on, the interior part of grains also feels more of a pressure, while the interface volumes are highly compressed. The importance conclusion is that the pressure is not a direct result of interfacail distortion, but a consequence of migration of the deformed interfaces.

The experimental measurements show that the interfacial stresses at the nanoscale structure can easily exceed 1GPa [115]. At the triple junctions one can see that this value can be remarkably larger (up to 40 times). Of course this occurs in a very short time, when the interfaces suddenly move and the instant mechanical deformation is

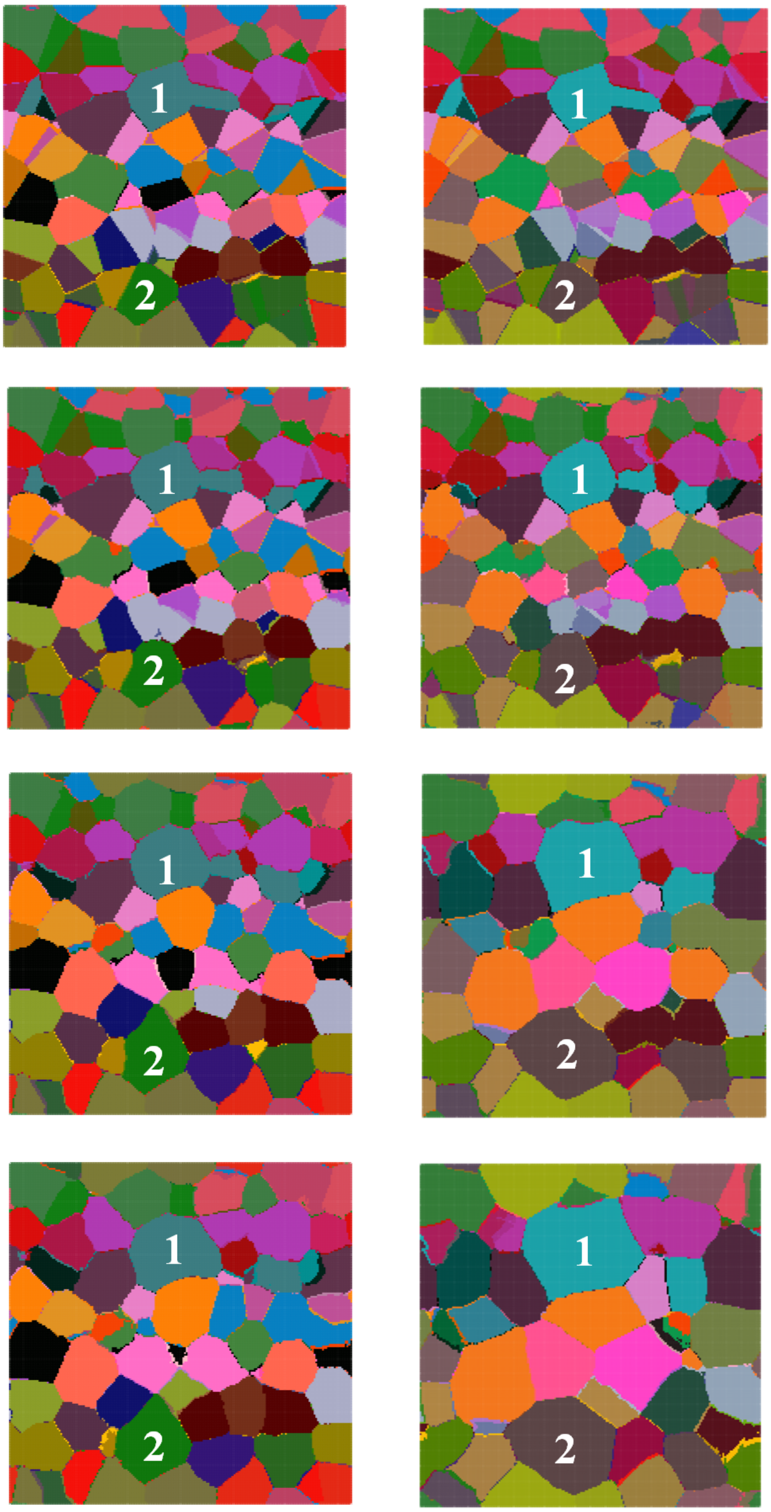

Figure 4.8: Cross section of simulation boxes for $10M_{a0}$ (left column) and $100M_{a0}$ (right column) atomic mobilities. The images in each row belong to the same time step (from top to below initial, 100s, 200s and 300s). The grains "1" and "2" can be clearly compared in two set of simulations.

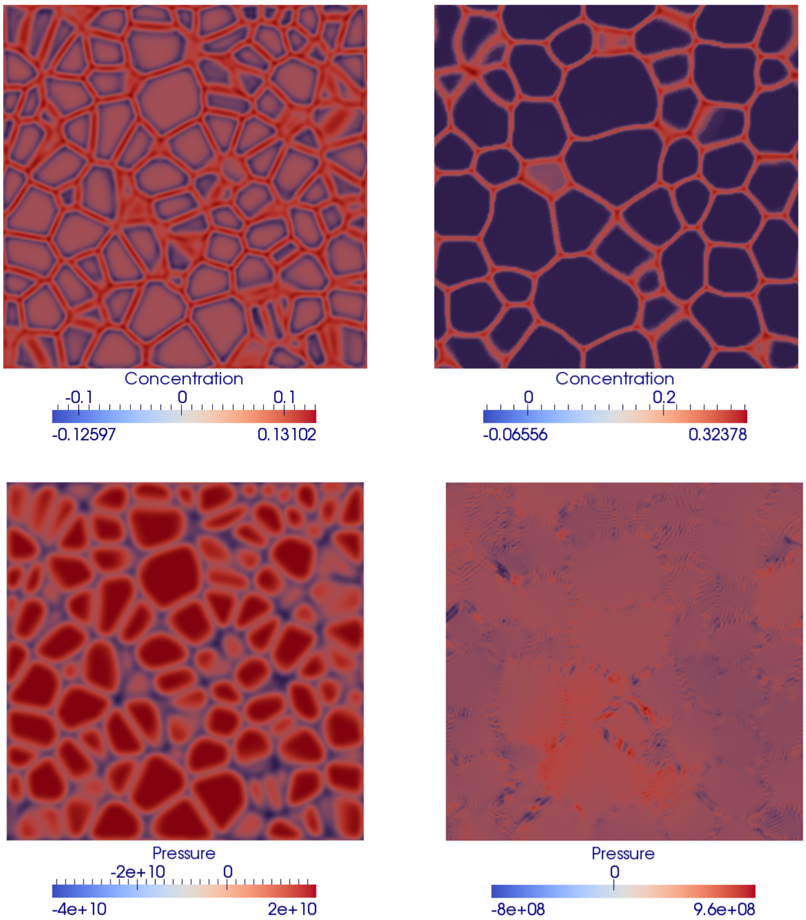

Figure 4.9: Concentration and pressure fields are compared for $10M_{a0}$ after 10 (left) and 1000s (right).

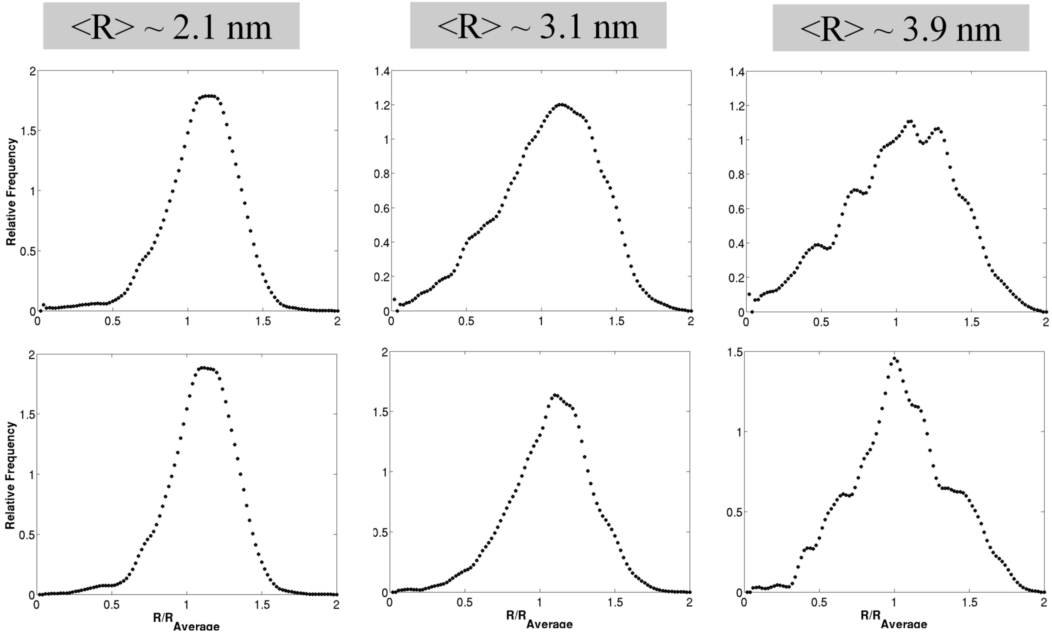

Figure 4.10: Size distribution for normal grain growth (top row) and diffusion-controlled grain growth (below row) at three different steps. For comparison, the distributions are presented for almost the same average grain sizes.

build up. Thereafter the amplitude of pressure decreases. Vacancies, however, can not catch the large stress gradients unless diffusion happens fast. At the later stages of the growth, when the diffusion and stress are almost balanced and their changes are small, the pressure is reduced and nearly equal over the system. In this step, the concentration is localized at the interfaces to relax the distortions as much as possible.

The grain size distributions were compared for diffusion-controlled regime in Figure 4.10. For better comparison, the distributions are presented for almost the same average grain sizes. Since statistics are pretty poor (limited number of grains), it is difficult to investigate whether transition to a self-similar regime for nanograin growth happens or how it may differ from normal regime of growth. However, the evolution of diffusion-controlled growth is distinguishable in general. At the nano-regime, tendency towards a rather narrow distribution is observed: population of the (relatively) small grains rapidly decline and a plateau forms in the left side of the graphs while the relative number of grains at the average-size remains intense. It seems that below a certain size, the curvature overcomes the mechanical barrier for motion. Another possibility is that the stress fields may neutralize each other through long-range interaction which is doable across the small grains.

4.8 Chapter conclusion

A phase-field model has been verified and applied for grain growth on the nanoscale in which the existence of extra interface volume possessing mechanical distortion is taken into account. The interaction between interfacial stress and vacancies, as mobile defects, introduce a new regime for dynamics and kinetics of the interfaces. The geometrically-required deformation at the interface builds mechanochemical potential gradient, the compensation of which seeks vacancies to diffuse-in from the adjacent volumes. Therefore, the kinetics of interfacial migration found to be controlled by balancing between diffusion of the vacancies, as well as the curvature of the interface. At low temperature, slow diffusion is the bottleneck of the grain growth which conducts low-speed linear growth regime on the nanoscale. At this stage, even the curvature driving force is substantial (small grain size) the motion of the interface is locked by mechanical distortion, the relaxation of which requires rapid diffusion. At high temperatures, however, the diffusion speeds up and meets the mechanical relaxation at interfaces. The growth, therefore, is curvature-driven in this condition. Between the two extreme cases, the balance between two controlling mechanisms determine the kinetics of the growth. Once the mobile defects can not catch the moving interface, an internal pressure is build up within the grains and grain boundaries proportional to the local density variation. This pressure is long-range and can contribute to the neighbouring grains and interfaces. It is observed that in this situation relatively small nanograins are very unstable and grains with the average grain size persist more than any other grains.

Appendix A

A Brief note on code developments

To accomplish present thesis, much effort has been made to create a new efficient and quick program which enable us to simulate the physical problems of interest. This code has been developed in C++ environment and has a modular structure, in which distinct classes for phase-field, concentration and elasticity are defined. Each class is meant to have its own local variables/functions as well as access to needed global variable and functions, and to be stored in a separate file. The classes also are coupled within specific functions to express special effects such as vacancy-stress relationship. The main() function then calls the initial functions (needed for reading inputs, initialization, memory reservation,...) and maintains main-loop which handles simulation steps and writing outputs (see flowchart Figure A.1). The results of current code developments are collected in OpenPhase [116], the open-source package for phase-field simulations. In the following I will give a brief explanation about the code structure and its developments.

A.1 Computation of derivatives

In MPF equations, time and space derivatives of phase-fields , concentrations and displacements are required. These contributions may interact with each other, depending on the problem during the computations. For example, the normal vectors to the interfaces computed in the phase-field space may be employed for any other events such as averaging of the driving forces, evaluation of the interface stiffness etc. Here I present few more details about derivatives.

Phase-field: The gradients of phase-fields are calculated using their first nearest neighbours and for their Laplacian, I apply an isotropic stencil with include 26 neighbours (first nearest neighbours plus diagonals) [66]. For time derivatives, an Eulerian finite difference scheme for both phase- and concentration fields is applied. The phase-fields are summed up with all other driving forces created by mechanical and diffusion contributions and updated in each time step. Phase-field computation is limited to the interfaces and their first neighbours.

Concentration field: For the concentration, a general diffusion function should be solved which requires chemical potentials as an input. In contrast to phase-fields, the

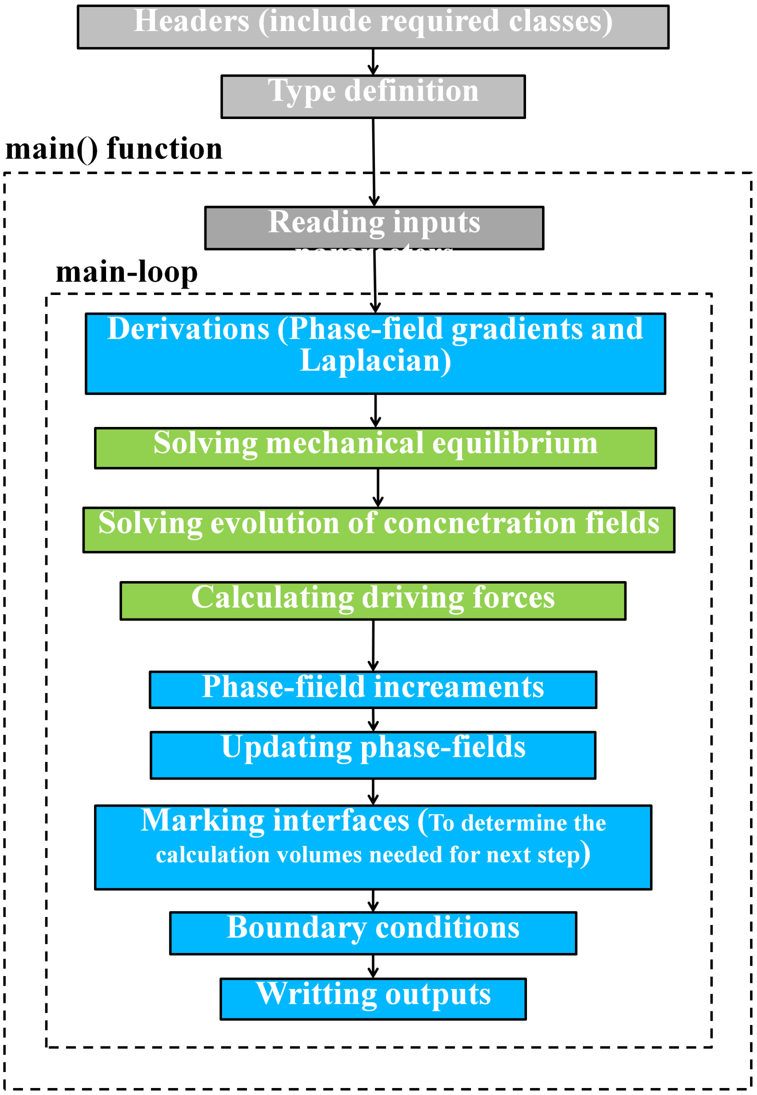
Headers (include required classes)
Type definition
main() function
Reading inputs
main-loop
Derivations (Phase-field gradients and Laplacian)
Solving mechanical equilibrium
Solving evolution of concnetration fields
Calculating driving forces
Phase-fiield increaments
Updating phase-fields
Marking interfaces (To determine the calculation volumes needed for next step)
Boundary conditions
Writting outputs

Figure A.1: Simple flowchart of computation algorithm.

concentration should be solved over whole simulation box. The time step of diffusion steps is usually small and the bottleneck against speed of the calculations.

Mechanical fields: Strains and stresses are the output of the mechanical solver. We use a spectral solver based on FFT method which is rather fast but limited to periodic boundary conditions. Its iterative scheme allows for tuning precision of the solution depending on the problem and the performance concerns. The grid points for mechanical solver match the phase-field grid points. Due to the symmetry, there are only 6 independent components for strain and stress at each point in the space, which is still a huge amount of data. derivatives of elastic energy can be input for both concentration and phase-fields classes.

A.2 Memory structure

One of the challenges for simulation studies presented here was the large amount of data which should be stored or written as output. This requires large amount of storage capacity as well as extra computation time for writing them. In the MPF model N phase-field variables are assigned to each point in the space requiring $N \times nX \times nY \times nZ$ units of the memory which is a large number in our simulations. Technically, however, the number of existing phases[1] at each point in space is much less than N and frequently there is only one phase (inside each domain). Therefore, we designed a dynamic storage algorithm which only stores the existing phase-fields but not all of them. This is handled using a C++ vector container which allows for easy resizing, looping, adding and deleting of each individual phase value(s), due to its pointing mechanism. A phase-field list contains C++ structures, each block having a phase number and its phase-field value. Thus, the size of the list is equal to the number of available phases. The schematic description is given in Figure A.2. In this way we succeed to increase the size of the simulation domain which was crucial for the studies of normal grain growth.

A.3 Inputs and outputs

All input parameters were read from an ASCII file which eases the interaction with the code. Each module has its own input file where only its relevant parameters are provided. The type of variables are mostly defined in a *Settings* class which take care of general input parameters. The phase-field variable is taken as float which is smaller than double (represented 32 bits against 64 bits) but still satisfies the expected accuracy. The concentrations, strains and stresses, however, should have a double precision.

For initialization input of big simulation boxes, Voro++ program [67] was partially modified and used. The domains have usually sharp interfaces at the beginning which should be carefully treated at the initial step of simulation. For other cases, initializations are written in individual predefined functions with diffuse interfaces.

Writing output is one of the time-consuming steps of the simulations. Reading/writing functions have been developed such that they gather minimum amount of data. Phase-field values, concentrations, stresses and strains were the general outputs of the simulations. In order to preserve accuracy, they were partially written/read

---

[1] In the phase-field simulations grains of the same material are distinguished by their local lattice orientation.

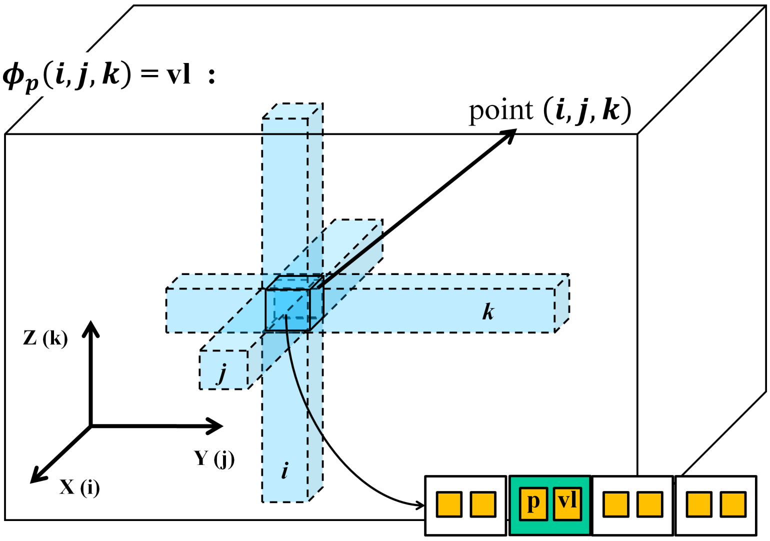

Figure A.2: Schematic demonstration of the storage structure of phase-fields. The phase-field value of phase p in the point (i, j, k) in the space is stored in a 3D vector of a structure. If the phase does not exist, the algorithm automatically returns the value 0.

in binary format and stored in separate files and named according to their respective time-step. In this way, it is easy to continue interrupted simulations. Phase-field outputs contain the number of phases and their values in all points of the domain. Outputs with "vtk" format were generated for visualization using Paraview software and the raw outputs feed the statistical analysis programs developed in MATLAB and C++.

Appendix B

Mechanical equilibrium around a deformed interface

I obtain analytical solutions for mechanical equilibrium around a deformed interface. The simple model depicted in Figure 4.2 considers a single spherical grain of radius R_A separated with a diffuse interface of width $R_B - R_A$ from an infinite substrate (domain C). Deformation of the interface is assumed to be only volumetric and reflected in its eigenstrains. The properties of three domains are denoted with indexes A, B and C. Assuming continuity of stress and displacement, the analytical solutions in spherical coordinate (r, θ, Φ) are given by

For $r < R_A$:

$$\sigma^{rr} = \frac{E_A}{(1+\nu)(1-2\nu)}\Big((1-\nu)(D_1 - \epsilon_A^{*rr}) + \nu(2D_1 - \epsilon_A^{*\theta\theta} - \epsilon_A^{*\Phi\Phi})\Big), \tag{B.1}$$

$$\sigma^{\theta\theta} = \frac{E_A}{(1+\nu)(1-2\nu)}\Big((1-\nu)(D_1 - \epsilon_A^{*\theta\theta}) + \nu(2D_1 - \epsilon_A^{*\theta\theta} - \epsilon_A^{*rr})\Big) \tag{B.2}$$

and

$$\sigma^{\Phi\Phi} = \frac{E_A}{(1+\nu)(1-2\nu)}\Big((1-\nu)(D_1 - \epsilon_A^{*\Phi\Phi}) + \nu(2D_1 - \epsilon_A^{*\theta\theta} - \epsilon_A^{*rr})\Big). \tag{B.3}$$

For $R_A \le r < R_B$:

$$\sigma^{rr} = \frac{E_B}{(1+\nu)(1-2\nu)}\left((1-\nu)(D_2 - \frac{2D_3}{r^3} - \epsilon_B^{*rr}) + \nu(2D_2 + \frac{2D_3}{r^3} - \epsilon_B^{*\theta\theta} - \epsilon_B^{*\Phi\Phi})\right), \tag{B.4}$$

$$\sigma^{\theta\theta} = \frac{E_B}{(1+\nu)(1-2\nu)}\left((1-\nu)(D_2+\frac{D_3}{r^3}-\epsilon_B^{*\theta\theta})+\nu(2D_2-\frac{2D_3}{r^3}-\epsilon_B^{*\Phi\Phi}-\epsilon_B^{*rr})\right) \tag{B.5}$$

and

$$\sigma^{\Phi\Phi} = \frac{E_B}{(1+\nu)(1-2\nu)}\left((1-\nu)(D_2+\frac{D_3}{r^3}-\epsilon_B^{*\Phi\Phi})+\nu(2D_2-\frac{2D_3}{r^3}-\epsilon_B^{*\theta\theta}-\epsilon_B^{*rr})\right). \tag{B.6}$$

For $r \geq R_B$:

$$\sigma^{rr} = \frac{E_C}{(1+\nu)(1-2\nu)}\left((1-\nu)(-\frac{2D_4}{r^3}-\epsilon_C^{*rr})+\nu(\frac{2D_4}{r^3}-\epsilon_C^{*\theta\theta}-\epsilon_C^{*\Phi\Phi})\right), \tag{B.7}$$

$$\sigma^{\theta\theta} = \frac{E_C}{(1+\nu)(1-2\nu)}\left((1-\nu)(\frac{2D_4}{r^3}-\epsilon_C^{*\theta\theta})+\nu(-\frac{D_4}{r^3}-\epsilon_C^{*\Phi\Phi}-\epsilon_C^{*rr})\right) \tag{B.8}$$

and

$$\sigma^{\Phi\Phi} = \frac{E_C}{(1+\nu)(1-2\nu)}\left((1-\nu)(\frac{D_4}{r^3}-\epsilon_C^{*\Phi\Phi})+\nu(-\frac{D_4}{r^3}-\epsilon_C^{*\theta\theta}-\epsilon_C^{*rr})\right). \tag{B.9}$$

In these equation D_1, D_2, D_3 and D_4 are constant :

$$\begin{aligned} D_1 &= \frac{P_2}{P_1}\left(-\frac{2E_C}{(1+\nu)R_B^3R_A^3}+\frac{E_B}{(1-2\nu)R_B^3R_A^3}+\frac{2E_C-2E_B}{(1+\nu)R_B^6}\right) \\ &\quad +\frac{P_3}{R_A^3R_B^3P_1}\left(\frac{2E_B}{(1+\nu)}-\frac{E_B}{(1-2\nu)}\right), \end{aligned} \tag{B.10}$$

$$D_2 = \frac{P_2}{R_B^6P_1}\left(\frac{2E_C-2E_B}{(1+\nu)}\right)+\frac{P_3}{R_A^3R_B^3P_1}\left(\frac{2E_B}{(1+\nu)}-\frac{E_A}{(1-2\nu)}\right), \tag{B.11}$$

$$D_3 = \frac{P_2}{R_B^3P_1}\left(-\frac{2E_C}{(1+\nu)}+\frac{E_B}{(1-2\nu)}\right)+\frac{P_3}{R_B^3P_1}\left(\frac{E_A-E_B}{(1-2\nu)}\right) \tag{B.12}$$

and

$$\begin{aligned} D_4 &= \frac{P_2}{R_B^3 P_1}\left(\frac{2E_B}{(1+\nu)} + \frac{E_B}{(1-2\nu)}\right) \\ &\quad + \frac{P_3}{P_1}\left(\frac{2E_B}{(1+\nu)R_A^3} - \frac{E_A}{(1-2\nu)R_A^3} + \frac{E_A - E_B}{(1-2\nu)R_B^3}\right) \end{aligned} \qquad \text{(B.13)}$$

where

$$\begin{aligned} P_1 &= \frac{E_A}{(1-2\nu)} \times \\ &\quad \left(\frac{1}{R_B^3}\left(\frac{2E_B}{(1+\nu)R_B^3} - \frac{E_B}{(1-2\nu)R_A^3}\right) + \frac{2E_C}{(1+\nu)R_B^3}\left(\frac{1}{R_A^3} - \frac{1}{R_B^3}\right)\right) \\ &\quad + \frac{2E_B}{(1+\nu)R_A^3 R_B^3}\left(\frac{2E_C}{(1+\nu)} - \frac{E_B}{(1-2\nu)}\right) + \frac{2E_B}{(1-2\nu)(1+\nu)R_B^6}\left(E_B - E_C\right), \end{aligned} \qquad \text{(B.14)}$$

$$\begin{aligned} P_2 &= \frac{1}{(1+\nu)(1-2\nu)} \times \\ &\quad \Big((1-\nu)(-E_B\epsilon_B^{*rr} + E_C\epsilon_C^{*rr}) - \nu E_B(\epsilon_B^{*\theta\theta} + \epsilon_B^{*\Phi\Phi}) + \nu E_A(\epsilon_A^{*\theta\theta} + \epsilon_A^{*\Phi\Phi})\Big) \end{aligned} \qquad \text{(B.15)}$$

and

$$\begin{aligned} P_3 &= \frac{1}{(1+\nu)(1-2\nu)} \times \\ &\quad \Big((1-\nu)(-E_B\epsilon_B^{*rr} + E_C\epsilon_C^{*rr}) - \nu E_B(\epsilon_B^{*\theta\theta} + \epsilon_B^{*\Phi\Phi}) + \nu E_C(\epsilon_C^{*\theta\theta} + \epsilon_C^{*\Phi\Phi})\Big). \end{aligned} \qquad \text{(B.16)}$$

The Young modulus for isotropic material is $E = \frac{C^{11}(1+\nu)(1-2\nu)}{1-\nu} = \frac{C^{12}(1+\nu)(1-2\nu)}{\nu} = 2(1+\nu)C^{44}$.

Appendix C

Homogenization methods at diffuse interfaces

Since phase-field is about multi-phases (grains) in contact, it should be combined with proper homogenization methods to satisfy the continuity conditions for stress and displacement. A few well-known methods which are relevant to our studies are briefly introduced here.

Voigt model In this model, it is assumed that the strain is uniform among all domains. This is true when two phases of similar stiffness are brought into contact. Applying this assumption into phase-field, the total strain at the diffuse interface considered to be equal (*Attention*: in this appendix I avoid the indexes for stress, strain and elastic constants to make the equations readable. Of course for demanding or unclear statements, I will explain them properly.):

$$\epsilon = \epsilon_\alpha = \epsilon_\beta, \tag{C.1}$$

and effective stress is expressed by weighting stresses of different phases,

$$\sigma = \phi_\alpha \sigma_\alpha + \phi_\beta \sigma_\beta = \phi_\alpha \bar{C}_\alpha (\epsilon - \epsilon^*_\alpha) + \phi_\beta \bar{C}_\beta (\epsilon - \epsilon^*_\beta). \tag{C.2}$$

Therefore the effective elastic constants and eigenstrains will be,

$$\bar{C}_{eff} = \phi_\alpha \bar{C}_\alpha + \phi_\beta \bar{C}_\beta, \tag{C.3}$$

$$\epsilon^*_{eff} = \bar{C}^{-1}_{eff} \left(\phi_\alpha \bar{C}_\alpha \epsilon^*_\alpha + \phi_\beta \bar{C}_\beta \epsilon^*_\beta \right). \tag{C.4}$$

The elastic energy stored in the system also can be described in the terms of effective parameters,

$$f^{mech} = \frac{1}{2}(\epsilon - \epsilon^*_{eff}) \bar{C}_{eff} (\epsilon - \epsilon^*_{eff}). \tag{C.5}$$

Reuss model If the phases in contact are very different in elastic moduli, they may expand or contract very differently against forces. In such case homogenizing of stresses within diffuse interface is rather useful,

$$\sigma = \sigma_\alpha = \sigma_\beta. \tag{C.6}$$

The strain can be averaged between two phases,

$$\epsilon = \phi_\alpha \epsilon_\alpha + \phi_\beta \epsilon_\beta = \phi_\alpha \bar{C}_\alpha^{-1} \sigma + \phi_\beta \bar{C}_\beta^{-1} \sigma. \tag{C.7}$$

The effective elastic constants and eigenstrains would be

$$\bar{C}_{eff} = \left(\phi_\alpha \bar{C}_\alpha^{-1} + \phi_\beta \bar{C}_\beta^{-1} \right)^{-1} \tag{C.8}$$

and

$$\epsilon^*_{eff} = \epsilon^*_\alpha = \epsilon^*_\beta. \tag{C.9}$$

Substituting these formulations into Equation C.5 the elastic energy density obtains.

Khachaturyan model In 1983 [35] Khachaturyan introduced a mixture model which takes weighted eigenstrain and elastic constants,

$$\epsilon^*_{eff} = \phi_\alpha \epsilon^*_\alpha + \phi_\beta \epsilon^*_\beta, \quad \bar{C}_{eff} = \phi_\alpha \bar{C}_\alpha + \phi_\beta \bar{C}_\beta. \tag{C.10}$$

The first assumption is similar to Reuss approach whereas the second assumption is a result of Voigt model. The stress is given by Hook's law as,

$$\sigma = \bar{C}_{eff}(\epsilon - \epsilon^*_{eff}) = (\phi_\alpha \bar{C}_\alpha + \phi_\beta \bar{C}_\beta)(\epsilon - \phi_\alpha \epsilon^*_\alpha - \phi_\beta \epsilon^*_\beta), \tag{C.11}$$

and the elastic energy obtains again by inserting these materials into Equation C.5. In contrary to two standard models above, the assumptions of Khachaturyan model does not allow for definition of phase elastic energy separately [117].

Steinbach model Steinbach et al. [3] proposed another approach, applicable for their MPF concept. They assumed uniform stress across diffuse interface, but they consider the elastic strain to be linearly weighted with phase-field variables,

$$\sigma = \sigma_\alpha = \sigma_\beta \tag{C.12}$$

and

$$\epsilon - \epsilon^* = \phi_\alpha(\epsilon_\alpha - \epsilon^*_\alpha) + \phi_\beta(\epsilon_\alpha - \epsilon^*_\alpha). \tag{C.13}$$

The effective elastic constants here are the same as Equation C.7 from Reuss approach, and the elastic energy is again as Equation C.5.

Appendix D

Averaging driving force over the interface

Discrete volumes in our numerical scheme may influence the accuracy of the computations. Even sometimes, it may produce artefacts and instabilities at the interface. For instance, if there is multi-extrema function acting on the interface area, the calculations may fail to catch some critical points or to miscalculate the overall contribution of driving forces.

In the model, presented in Chapter 4, the driving force due to geometrically-required eigenstrains builds a two extrema function with large range but small average value. This is shown schematically in Figure D.1. Since the local values are so divers, the interface may be very unstable. In order to avoid these effects, I average the driving forces at the interface and redistribute them by a rather smooth function.

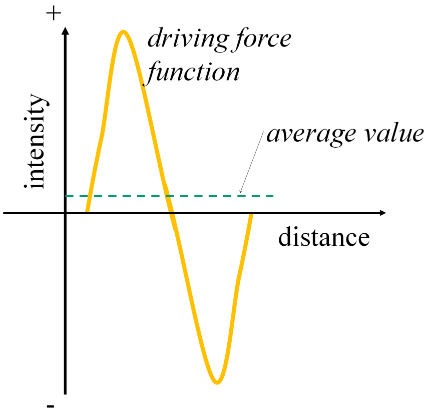

Figure D.1: Schematic sketch of driving force function over an 1D interface (see Section 4.5.2). The total average value is much smaller than extrema.

Averaging should be done in the normal direction over the surface or line of the interface defined as $\frac{|\nabla\phi|}{\nabla\phi}$. For averaging, theoretically one should integrate the values along the normal vector and divide by its length. In a discrete space, however, any

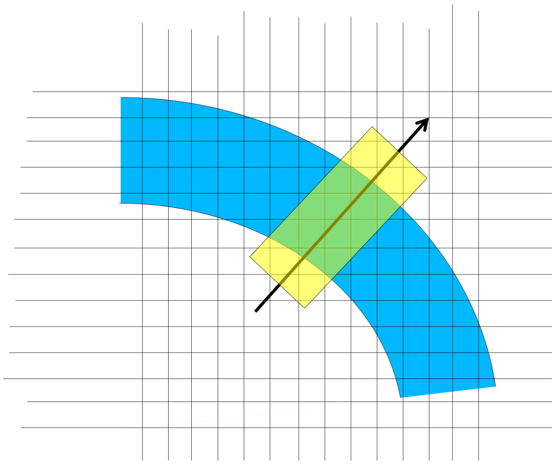

Figure D.2: 2D Schematic expression of the averaging. The rectangular (cylinder in 3D) over the interface (curved area) is parallel to the normal vector plotted for a certain point at the centre of the interface.

defined vector may hit randomly some grid points. This is not numerically enough accurate, especially for averaging over heterogeneously distributed values. To resolve this issue, a certain distance around normal vector are attributed to it such that it covers all its nearest neighbours. This is similar to averaging over values inside a cylinder for which its axis is coincide with the normal vector. Figure D.2 gives graphical explanation for this method. Thus, the average value should be redistributed using a proper function over the interface. Two typical non-zero function are $\frac{8}{\eta}\phi(1-\phi)$ or $\frac{\pi}{\eta}\sqrt{\phi(1-\phi)}$, the integration of which over the profile of an interface with DO potential is equal to 1.

References

[1] M. Hillert. **On the theory of normal and abnormal grain growth**. *Acta Metallurgica*, **13**(3):227 – 238, 1965. v, 19, 28, 42, 44

[2] I. Steinbach. **Phase-field models in materials science**. *Modelling and Simulation in Materials Science and Engineering*, **17**(7):073001, 2009. vii, 4, 8, 10

[3] I. Steinbach and M. Apel. **Multi phase field model for solid state transformation with elastic strain**. *Physica D: Nonlinear Phenomena*, **217**(2):153 – 160, 2006. vii, 10, 92

[4] P.R. Rios and M.E. Glicksman. **Polyhedral model for self-similar grain growth**. *Acta Materialia*, **56**(5):1165 – 1171, 2008. vii, 22, 33, 38, 42

[5] E.A. Lazar, J.K. Mason, R.D. MacPherson, and D.J. Srolovitz. **A more accurate three-dimensional grain growth algorithm**. *Acta Materialia*, **59**(17):6837 – 6847, 2011. vii, 38, 42

[6] X. Song, K. Yang, and J. Zhang. **Incontinuous Grain Growth in Cobalt Nanocrystalline Powders Prepared by High-Energy Mechanical Milling**. *Journal of Nanoscience and Nanotechnology*, **5**(12):2155 – 2160, 2005. x, 65, 78

[7] C.E. Krill, L. Helfen, D. Michels, H. Natter, A. Fitch, O. Masson, and R. Birringer. **Size-Dependent Grain-Growth Kinetics Observed in Nanocrystalline Fe**. *Physical Review Letter*, **86**:842 – 845, 2001. x, 76

[8] R.W. Cahn and P. Haasen. *Physical metallurgy*. Elsevier Science, 1996. 2

[9] B. Zhao, G. Gottstein, and L.S. Shvindlerman. **Triple junction effects in solids**. *Acta Materialia*, **59**(9):3510 – 3518, 2011. 4

[10] U. Czubayko, V.G. Sursaeva, G. Gottstein, and L.S. Shvindlerman. **Influence of triple junctions on grain boundary motion**. *Acta Materialia*, **46**(16):5863 – 5871, 1998. 4

[11] M. Hillert. **Impact of Clarence Zener upon metallurgy**. *Journal of Applied Physics*, **60**(6):1868–1876, 1986. 4

[12] P.A. Manohar, M. Ferry, and T. Chandra. **Five Decades of the Zener Equation**. *ISIJ International*, **38**(9):913 – 924, 1998. 4, 47

[13] P.M. Hazzledine and R.D.J. Oldershaw. **Computer simulation of Zener pinning**. *Philosophical Magazine A*, **61**(4):579 – 589, 1990. 4, 47

[14] M. Hillert. **Inhibition of grain growth by second-phase particles**. *Acta Metallurgica*, **36**(12):3177 – 3181, 1988. 4, 47

[15] J.W. Gibbs and P. Haasen. *The collected works of J. Willard Gibbs*. Longmans, Green and Co., 1902. 4

[16] W.J. Boettinger, J.A. Warren, C. Beckermann, and A. Karma. **PHASE-FIELD SIMULATION OF SOLIDIFICATION**. *Annual Review of Materials Research*, **32**(1):163 – 194, 2002. 6, 8

[17] J.W. Cahn and J.E. Hilliard. **Free Energy of a Nonuniform System. I. Interfacial Free Energy**. *The Journal of Chemical Physics*, **28**(2):258 – 267, 1958. 6

[18] S.M. Allen and J.W. Cahn. **A microscopic theory for antiphase boundary motion and its application to antiphase domain coarsening**. *Acta Metallurgica*, **27**(6):1085 – 1095, 1979. 6, 7

[19] S.-K. Chan. **Steady-state kinetics of diffusionless first order phase transformations**. *The Journal of Chemical Physics*, **67**(12):5755 – 5762, 1977. 7

[20] G. Caginalp. **Phase Field Models and Sharp Interface Limits: Some Differences in Subtle Situations**. *Rocky Mountain Journal of Mathematics*, **21**(2):603–615, 1991. 7

[21] S.-L. Wang, R.F. Sekerka, A.A. Wheeler, B.T. Murray, S.R. Coriell, R.J. Braun, and G.B. McFadden. **Thermodynamically-consistent phase-field models for solidification**. *Physica D: Nonlinear Phenomena*, **69**(12):189 – 200, 1993. 7

[22] A.A. Wheeler, W.J. Boettinger, and G.B. McFadden. **Phase-field model of solute trapping during solidification**. *Physical Review E*, **47**:1893 – 1909, 1993. 7

[23] N.A. Ahmad, A.A. Wheeler, W.J. Boettinger, and G.B. McFadden. **Solute trapping and solute drag in a phase-field model of rapid solidification**. *Physical Review E*, **58**:3436 – 3450, 1998. 8

[24] A. Karma and W.-J. Rappel. **Numerical Simulation of Three-Dimensional Dendritic Growth**. *Physical Review Letter*, **77**:4050 – 4053, 1996. 8

[25] A. Karma. **Phase-Field Formulation for Quantitative Modeling of Alloy Solidification**. *Physical Review Letter*, **87**:115701, 2001. 8

[26] R. Kobayashi. **Modeling and numerical simulations of dendritic crystal growth**. *Physica D: Nonlinear Phenomena*, **63**(34):410 – 423, 1993. 8

[27] R. Kobayashi. **A numerical approach to three-dimensional dendritic solidification**. *Exprimental Mathematics*, **3**(1):59 – 81, 1994. 8

[28] C. Beckermann, H.-J. Diepers, I. Steinbach, A. Karma, and X. Tong. **Modeling Melt Convection in Phase-Field Simulations of Solidification**. *Journal of Computational Physics*, **154**(2):468 – 496, 1999. 8

[29] B. Morin, K.R. Elder, M. Sutton, and M. Grant. **Model of the Kinetics of Polymorphous Crystallization**. *Physical Review Letter*, **75**:2156 – 2159, 1995. 8

[30] L.-Q. Chen and W. Yang. **Computer simulation of the domain dynamics of a quenched system with a large number of nonconserved order parameters: The grain-growth kinetics**. *Physical Review B*, **50**:15752 – 15756, 1994. 8

[31] R. Kobayashi, J.A. Warren, and W.C. Carter. **A continuum model of grain boundaries**. *Physica D: Nonlinear Phenomena*, **140**(12):141 – 150, 2000. 9

[32] I. Steinbach, F. Pezzolla, B. Nestler, M. Seeelberg, R. Prieler, G.J. Schmitz, and J.L.L. Rezende. **A phase field concept for multiphase systems**. *Physica D: Nonlinear Phenomena*, **94**(3):135 – 147, 1996. 9

[33] J. Tiaden, B. Nestler, H.J. Diepers, and I. Steinbach. **The multiphase-field model with an integrated concept for modelling solute diffusion**. *Physica D: Nonlinear Phenomena*, **115**(12):73 – 86, 1998. 9

[34] F.C. Larche and J.l. Cahn. **The effect of self-stress on diffusion in solids**. *Acta Metallurgica*, **30**(10):1835 – 1845, 1982. 10, 64

[35] A. Khachaturyan. *Theory of phase transformation in solids.* John Wiley & Sons, 1983. 10, 64, 92

[36] I. Steinbach and F. Pezzolla. **A generalized field method for multiphase transformations using interface fields**. *Physica D: Nonlinear Phenomena*, **134**(4):385 – 393, 1999. 10, 14

[37] L.V. Mikheev and A.A. Chernov. **Mobility of a diffuse simple crystalmelt interface**. *Journal of Crystal Growth*, **112**(23):591 – 596, 1991. 11

[38] *Metal interfaces: a seminar on metal interfaces held during the Thirty-third National Metal Congress and Exposition.* American Society for Metals, 1951. 13

[39] T. Young. **An Essay on the Cohesion of Fluids**. *Philosophical Transactions of the Royal Society of London*, **95**:65 – 87, 1805. 13, 16, 17

[40] P. Blikstein and A.P. Tschiptschin. **Monte Carlo simulation of grain growth**. *Materials Research*, **2**:133 – 137, 1999. 13

[41] F. Wakai, N. Enomoto, and H. Ogawa. **Three-dimensional microstructural evolution in ideal grain growthgeneral statistics**. *Acta Materialia*, **48**(6):1297 – 1311, 2000. 13, 38, 42

[42] H.J. Frost and C.V. Thompson. **Computer simulation of grain growth**. *Current Opinion in Solid State and Materials Science*, **1**(3):361 – 368, 1996. 13

[43] D. Weygand, Y. Brechet, and J. Lepinoux. **A vertex dynamics simulation of grain growth in two dimensions**. *Philosophical Magazine Part B*, **78**(4):329 – 352, 1998. 13

[44] Y. Liu, T. Baudin, and R. Penelle. **Simulation of normal grain growth by cellular automata**. *Scripta Materialia*, **34**(11):1679 – 1683, 1996. 13

[45] D. Fan and L.-Q. Chen. **Computer simulation of grain growth using a continuum field model**. *Acta Materialia*, **45**(2):611 – 622, 1997. 13

[46] C.E. Krill III and L.-Q. Chen. **Computer simulation of 3-D grain growth using a phase-field model**. *Acta Materialia*, **50**(12):3059 – 3075, 2002. 13

[47] J.E. Burke and D. Turnbull. **Recrystallization and grain growth**. *Progress in Metal Physics*, **3**(0):220 – 292, 1952. 13, 17

[48] W.W. Mullins. **Two-Dimensional Motion of Idealized Grain Boundaries**. *Journal of Applied Physics*, **27**(8):900 – 904, 1956. 14

[49] H.V. Atkinson. **Overview no. 65: Theories of normal grain growth in pure single phase systems**. *Acta Metallurgica*, **36**(3):469 – 491, 1988. 14

[50] W.W. Mullins. **Estimation of the geometrical rate constant in idealized three dimensional grain growth**. *Acta Metallurgica*, **37**(11):2979 – 2984, 1989. 14, 20, 37, 38

[51] S. Hilgenfeldt, A.M. Kraynik, S.A. Koehler, and H.A. Stone. **An**

Accurate von Neumann's Law for Three-Dimensional Foams. *Physical Review Letter*, **86**:2685 – 2688, 2001. 14, 21, 37, 38

[52] R.D. MacPherson and D.J. Srolovitz. **The von Neumann relation generalized to coarsening of three-dimensional microstructures**. *Nature*, **446**:1053 – 1055, 2007. 14, 21, 33, 38

[53] W.W. Mullins. **The statistical self-similarity hypothesis in grain growth and particle coarsening**. *Journal of Applied Physics*, **59**(4):1341 – 1349, 1986. 14

[54] W. Guo and I. Steinbach. **Multi-phase field study of the equilibrium state of multi-junctions**. *International Journal of Materials Research*, **101**(4):480 – 485, 2010. 14, 25

[55] W. Guo, R. Spatschek, and I. Steinbach. **An analytical study of the static state of multi-junctions in a multi-phase field model**. *Physica D: Nonlinear Phenomena*, **240**(45):382 – 388, 2011. 14

[56] R. Darvishi Kamachali and I. Steinbach. **3-D phase-field simulation of grain growth: Topological analysis versus mean-field approximations**. *Acta Materialia*, **60**(67):2719 – 2728, 2012. 14

[57] D.A. Porter and K.E. Easterling. *Phase Transformations in Metals and Alloys*. Taylor & Francis, 1992. 16

[58] P. Feltham. **Grain growth in metals**. *Acta Metallurgica*, **5**(2):97 – 105, 1957. 18, 38

[59] I.M. Lifshitz and V.V. Slyozov. **The kinetics of precipitation from supersaturated solid solutions**. *Journal of Physics and Chemistry of Solids*, **19**(12):35 – 50, 1961. 19

[60] K. Lucke, I. Heckelmann, and G. Abbruzzese. **Statistical theory of two-dimensional grain growthII. Kinetics of grain growth**. *Acta Metallurgica et Materialia*, **40**(3):533 – 542, 1992. 20

[61] N.P. Louat and M.S. Duesbery. **On the theory of normal grain growth**. *Philosophical Magazine A*, **69**(5):841 – 854, 1994. 20

[62] C.S. Pande. **On a stochastic theory of grain growth**. *Acta Metallurgica*, **35**(11):2671 – 2678, 1987. 20

[63] M.E. Glicksman. **Analysis of 3-D network structures**. *Philosophical Magazine*, **85**(1):3 – 31, 2005. 21

[64] P.R. Rios and M.E. Glicksman. **Self-similar evolution of network structures**. *Acta Materialia*, **54**(4):1041 – 1051, 2006. 21, 38

[65] P.R. Rios and M.E. Glicksman. **Topological and metrical analysis of normal grain growth in three dimensions**. *Acta Materialia*, **55**(5):1565 – 1571, 2007. 22

[66] M. Patra and M. Karttunen. **Stencils with isotropic discretization error for differential operators**. *Numerical Methods for Partial Differential Equations*, **22**(4):936–953, 2006. 24, 84

[67] C.H. Rycroft. **VORO++: A three-dimensional Voronoi cell library in C++**. *Chaos: An Interdisciplinary Journal of Nonlinear Science*, **19**(4):041111, 2009. 27, 86

[68] S.G. Kim, D.I. Kim, W.T. Kim, and Y.B. Park. **Computer simulations of two-dimensional and three-dimensional ideal grain growth**. *Physical Review E*, **74**:061605, 2006. 31

[69] L.A. Barrales Mora, G. Gottstein, and L.S. Shvindlerman. **Three-dimensional grain growth: Analytical approaches and computer simulations**. *Acta Materialia*, **56**(20):5915 – 5926, 2008. 34

[70] G. Gottstein, A.H. King, and L.S. Shvindlerman. **The effect of triple-junction drag on grain growth**. *Acta Materialia*, **48**(2):397 – 403, 2000. 37

[71] K. Song and M. Aindow. **Grain growth and particle pinning in a model Ni-based superalloy**. *Materials Science and Engineering: A*, **479**(12):365 – 372, 2008. 44

[72] R.L. Higginson, M. Aindow, and P.S. Bate. **The effect of finely dispersed particles on primary recrystallisation textures in AlMnSi alloys**. *Materials Science and Engineering: A*, **225**(12):9 – 21, 1997. 44

[73] M.J. Jones and F.J. Humphreys. **Interaction of recrystallization and precipitation: The effect of Al3Sc on the recrystallization behaviour of deformed aluminium**. *Acta Materialia*, **51**(8):2149 – 2159, 2003. 44

[74] O. Kwon and A.J. DeArdo. **Interactions between recrystallization and precipitation in hot-deformed microalloyed steels**. *Acta Metallurgica et Materialia*, **39**(4):529 – 538, 1991. 44

[75] E. Palmiere, C. Garcia, and A. DeArdo. **The influence of niobium supersaturation in austenite on the static recrystallization behavior of low carbon microalloyed steels**. *Metallurgical and Materials Transactions A*, **27**:951 – 960, 1996. 44

[76] T. Gladman. **On the Theory of the Effect of Precipitate Particles on Grain Growth in Metals**. *Proceedings of the Royal Society of London. Series A, Mathematical and Physical Sciences*, **294**(438):298 – 309, 1966. 46

[77] E. Nes, N. Ryum, and O. Hunderi. **On the Zener drag**. *Acta Metallurgica*, **33**(1):11 – 22, 1985. 47

[78] N. Ryum, O. Hunderi, and E. Nes. **On grain boundary drag from second phase particles**. *Scripta Metallurgica*, **17**(11):1281 – 1283, 1983. 47, 57

[79] O. Hunderi, E. Nes, and N. Ryum. **On the zener dragAddendum**. *Acta Metallurgica*, **37**(1):129 – 133, 1989. 47

[80] S.P. Ringer, W.B. Li, and K.E. Easterling. **On the interaction and pinning of grain boundaries by cubic shaped precipitate particles**. *Acta Metallurgica*, **37**(3):831 – 841, 1989. 47, 57

[81] I. Steinbach and M. Apel. **Dual scale simulation of grain growh using multi phase field model**. *Material Research Society Symposium Proceeding*, **677:AA 7.14.1.**, 2001. 56

[82] M. Hillert and G.R. Purdy. **Chemically induced grain boundary migration**. *Acta Metallurgica*, **26**(2):333 – 340, 1978. 63, 65

[83] M. Hillert. **On the driving force for diffusion induced grain boundary migration**. *Scripta Metallurgica*, **17**(2):237 – 240, 1983. 63

[84] O. Penrose. **On the elastic driving force in diffusion-induced grain boundary motion**. *Acta Materialia*, **52**(13):3901 – 3910, 2004. 63

[85] R.W. Balluffi and J.W. Cahn. **Mechanism for diffusion induced grain boundary migration**. *Acta Metallurgica*, **29**(3):493 – 500, 1981. 64

[86] G. Schmitz, C.-B. Ene, and C. Nowak. **Reactive diffusion in nanostructures of spherical symmetry**. *Acta Materialia*, **57**(9):2673 – 2683, 2009. 64

[87] Z. Erdelyi and G. Schmitz. **Reactive diffusion and stresses in spherical geometry**. *Acta Materialia*, **60**(4):1807 – 1817, 2012. 64

[88] I. Steinbach, X. Song, and A. Hartmaier. **Phase-field model with plastic flow for grain growth in nanocrystalline material**. *Philosophical Magazine*, **90**(1-4):485 – 499, 2010. 64

[89] L. Lochte, A. Gitt, G. Gottstein, and I. Hurtado. **Simulation of the evolution of GP zones in AlCu alloys: an extended Cahn-Hilliard approach**. *Acta Materialia*, **48**(11):2969 – 2984, 2000. 64

[90] N. Zhou, C. Shen, M.F.-X. Wagner, G. Eggeler, M.J. Mills, and Y. Wang. **Effect of Ni4Ti3 precipitation on martensitic transformation in TiNi**. *Acta Materialia*, **58**(20):6685 – 6694, 2010. 64

[91] K.S. Kumar, H. Van Swygenhoven, and S. Suresh. **Mechanical behavior of nanocrystalline metals and alloys**. *Acta Materialia*, **51**(19):5743 – 5774, 2003. 65

[92] B.Q. Han, E.J. Lavernia, and F.A. Mohamed. **Mechanical properties of nanostructured materials**. *Reviews On Advanced Materials Science*, **9**(1):1 – 16, 2005. 65

[93] D. Wolf, V. Yamakov, S.R. Phillpot, A. Mukherjee, and H. Gleiter. **Deformation of nanocrystalline materials by molecular-dynamics simulation: relationship to experiments?** *Acta Materialia*, **53**(1):1 – 40, 2005. 65

[94] H. Gleiter. **Nanocrystalline materials**. *Progress in Materials Science*, **33**(4):223 – 315, 1989. 65

[95] H. Gleiter. **Nanostructured materials: basic concepts and microstructure**. *Acta Materialia*, **48**(1):1 – 29, 2000. 65

[96] I.A. Ovidko. **Nanodefects in nanostructures**. *Philosophical Magazine Letters*, **83**(10):611 – 620, 2003. 65

[97] T.R. Malow and C.C. Koch. **Grain growth in nanocrystalline iron prepared by mechanical attrition**. *Acta Materialia*, **45**(5):2177 – 2186, 1997. 65

[98] M. Ames, J. Markmann, R. Karos, A. Michels, A. Tschpe, and R. Birringer. **Unraveling the nature of room temperature grain growth in nanocrystalline materials**. *Acta Materialia*, **56**(16):4255 – 4266, 2008. 65

[99] J.H. Driver. **Stability of nanostructured metals and alloys**. *Scripta Materialia*, **51**(8):819 – 823, 2004. 65

[100] F. Ebrahimi and H. Li. **Grain growth in electrodeposited nanocrystalline fcc NiFe alloys**. *Scripta Materialia*, **55**(3):263 – 266, 2006. 65

[101] A.J. Haslam, S.R. Phillpot, D. Wolf, D. Moldovan, and H. Gleiter. **Mechanisms of grain growth in nanocrystalline fcc metals by molecular-dynamics simulation**. *Materials Science and Engineering: A*, **318**(12):293 – 312, 2001. 65

[102] M. Upmanyu, D.J. Srolovitz, L.S. Shvindlerman, and G Gottstein. **Molecular dynamics simulation of**

triple junction migration. *Acta Materialia*, **50**(6):1405 – 1420, 2002. 65

[103] D. Zollner. **A Potts model for junction limited grain growth**. *Computational Materials Science*, **50**(9):2712 – 2719, 2011. 65

[104] Y. Estrin, G. Gottstein, and L.S. Shvindlerman. **Inhibition of void dissolution by vacancies**. *Scripta Materialia*, **41**(4):415 – 420, 1999. 65, 76

[105] Y. Estrin, G. Gottstein, and L.S. Shvindlerman. **Intermittent self-locking of grain growth in fine-grained materials**. *Scripta Materialia*, **41**(4):385 – 390, 1999. 65, 76

[106] R. Sahara, T. Shishido, A. Nomura, K. Kudou, Sh. Okada, V. Kumar, K. Nakajima, and Y. Kawazoe. **Mechanism of the increase in bulk modulus of perovskite $ScRh_3B_x$ by vacancies**. *Physical Review B*, **73**:184102, May 2006. 66

[107] Y. Estrin, G. Gottstein, E.R., and L.S. Shvindlerman. **On the kinetics of grain growth inhibited by vacancy generation**. *Scripta Materialia*, **43**(2):141 – 147, 2000. 67, 76, 78

[108] Y. Estrin, G. Gottstein, E. Rabkin, and L.S. Shvindlerman. **Grain growth in thin metallic films**. *Acta Materialia*, **49**(4):673 – 681, 2001. 76

[109] L.S. Shvindlerman and R.G. Faulkner. **Thermodynamics of Vacancies and Impurities at Grain Boundaries**. *Interface Science*, **6**:213 – 224, 1998. 76

[110] L. Zhang, Y. Du, Y. Ouyang, H. Xu, X.-G. Lu, Y. Liu, Y. Kong, and J. Wang. **Atomic mobilities, diffusivities and simulation of diffusion growth in the CoSi system**. *Acta Materialia*, **56**(15):3940 – 3950, 2008. 78

[111] R. Darvishi Kamachali, J. Hua, I. Steinbach, and A. Hartmaier. **Multiscale simulations on the grain growth process in nanostructured materials**. *International Journal of Materials Research*, **11**(101):1332 – 1338, 2010. 79

[112] M. Chauhan and F.A. Mohamed. **Investigation of low temperature thermal stability in bulk nanocrystalline Ni**. *Materials Science and Engineering: A*, **427**(12):7 – 15, 2006. 79

[113] J. Wang, Y. Iwahashi, Z. Horita, M. Furukawa, M. Nemoto, R.Z. Valiev, and T.G. Langdon. **An investigation of microstructural stability in an AlMg alloy with submicrometer grain size**. *Acta Materialia*, **44**(7):2973 – 2982, 1996. 79

[114] J. Lian, R.Z. Valiev, and B. Baudelet. **On the enhanced grain growth in ultrafine grained metals**. *Acta Metallurgica et Materialia*, **43**(11):4165 – 4170, 1995. 79

[115] P. Zimmer and R. Birringer. **Measuring the interface stress of nanocrystalline iron**. *Applied Physics Letters*, **92**(8):081912, 2008. 79

[116] **www.openphase.de**. 84

[117] K. Ammar, B. Appolaire, G. Cailletaud, and S. Forest. **Combining phase field approach and homogenization methods for modelling phase transformation in elastoplastic media**. *European Journal of Computational Mechanics/Revue Europenne de Mcanique Numrique*, **18**(5-6):485 – 523, 2009. 92